CORAL EXTENSION RATE ANALYSIS USING COMPUTED AXIAL TOMOGRAPHY

A Thesis

by

ELEANOR ANN YUDELMAN

Submitted to the Office of Graduate and Professional Studies of
Texas A&M University
in partial fulfillment of the requirements for the degree of

MASTER OF SCIENCE

Chair of Committee,	Niall Slowey
Committee Members,	Deborah Thomas
	Benjamin Giese
	George P. Schmahl
Head of Department,	Deborah Thomas

May 2014

Major Subject: Oceanography

ABSTRACT

Biological and geological studies of coral reefs often rely on measured Scleractinian coral skeletal extension rates. Ideally, corallites are oriented parallel to a coral core's longitudinal axis and perpendicular to its annual high-density growth bands. To examine corallite orientations, we use high-resolution computed axial tomography to image ten short *Montastrea faveolata* cores from the northwest Gulf of Mexico. This non-destructive method enable the comparison of extension rates determined several ways: 1) across a single slice or slab X-ray image, 2) between 0.6 mm slice and 8.4mm slab X-ray images, and 3) among slice/slab orientated at varied angles relative to a coral core's longitudinal axis. Additionally, the true three-dimensional extension rate of individual corallites is determined and compared to the extension rate apparent on a two-dimensional slice/slab. Results suggest minimal significant differences between all methods, confirming the conventional extension rate methodology is suitable for studies if the core's longitudinal axis is in approximate alignment with the growth axis of the corallites. Determination of three-dimensional corallite growth patterns leads to improved understanding of the development of the coral colony.

DEDICATION

This is dedicated to my Grandparents who always pushed me to further my education and to my Parents for their unconditional love and support.

"Twenty years from now you will be more disappointed by the things you didn't do than by the ones you did do. So throw off the bowlines. Sail away from the safe harbor. Catch the trade winds in your sails. Explore. Dream. Discover." - Mark Twain

ACKNOWLEDGMENTS

I would like to first thank my advisor Dr. Niall Slowey, without whose support and guidance none of this would be possible. Thank you so much for all of your help over the past two years, I have truly enjoyed working with you and I greatly appreciate your friendship. Also my three committee members Dr. Debbie Thomas, Dr. Ben Geise and G.P. Schmahl, thank you for all of your help and advice during this process, I value your opinions very highly and appreciate your input.

My funding and support is provided by: The State of Texas Norman Hackerman Advanced Research Program, NOAA Flower Garden Banks National Marine Sanctuary, NSF-STEM Scholarship, Louis and Elizabeth Scherck Endowment Fellowship, and The Department of Oceanography at Texas A&M University.

Thank you to the TAMU Veterinary School for all the help with my cores, especially Hollye Callis for countless hours of CT scanning and computer manipulations. Thank you to the NOAA divers who collected and provided the cores and details of their collection. Thank you to Dr. Wormuth for helping me with my statistical analyses. Thank you to Amy, Wendy, Lisa and Missy for always knowing how to fix problems and keep everything in order. Thank you to all of my professors at Texas A&M University, I have learned a great deal over the past few years and can't wait to continue the journey.

Most importantly, thank you to my family for all of the encouragement and help throughout graduate school; I would not have been able to do it without you all. Especially my Mom, Dad, Emma, Adam and Bob for listening to me along the way and

always believing in me through thick and thin. Last but not least, thank you to all of my friends, near and far. Without all of you I would have never become the person I am today, and I greatly cherish all you have done for me.

NOMENCLATURE

FGNMS	Flower Gardens National Marine Sanctuary
NOAA	National Oceanographic and Atmospheric Administration
WFGB	West Flower Garden Bank
EFGB	East Flower Garden Bank
CT	Computed Axial Tomography
SCUBA	Self Contained Underwater Breathing Apparatus
ROI	Region of Interest
NE	Northeast
NW	Northwest
SE	Southeast
SW	Southwest
mm	Milimeters
cm	Centimeters
m	Meters
yr	Year

TABLE OF CONTENTS

Page

LIST OF FIGURES

FIGURE Page

LIST OF TABLES

1. INTRODUCTION

Shallow-water coral reef systems are some of the largest structures created by organisms and generally thought to serve as habitat for 25% of all marine species. These reefs also provide coastal protection, fisheries, pharmaceuticals, tourism, and other important resources to people (e.g., Lough 2008, Schmahl et al. 2008). The calcareous skeletons of scleractinian (hard) corals form the structural framework of the reefs (e.g. Milliman 1974, Wilson 1975, Vernon 2000a) moreover; these corals have proven to be sensitive monitors of ambient environmental conditions and regional climate via variations in their skeletal growth rate and chemical composition (review by Dunbar and Cole 1993, and references therein). Coral reefs worldwide are under stress because of human activities and climate change (e.g. Hughes et al. 2003; Pandolfi et al. 2003; Carpenter et al. 2008; Lough 2008) and the reefs in the Gulf of Mexico and Caribbean Sea region have declined markedly during the past several decades (e.g. Gardner et al. 2003; Burke and Maidens 2004; Wilkinson 2008; Kwiatkowski et al. 2013). To assess how the changes in these factors affects the vitality of coral reefs and reconstruct the history of climatic and other environmental conditions, it is important to determine the skeletal development of scleractinian corals.

The study of growth in calcareous hard parts is known as sclerochronology, this encompasses, but is not limited to, corals, mollusks, fish etc. (Buddemeier et al. 1974, Milliman 1974). Like dendrochronology (the study of tree rings), coral sclerochronology enables biological and geological changes within an environment to be recorded (Buddemeier et al. 1974, Hudson et al. 1976) either in terms of chronological or

geochemical records (e.g. Lough and Barnes 1990, Lough and Cooper 2011). Chronological studies define coral growth in terms of skeletal density, extension rates, and calcification rates. Geochemical studies use the elemental and isotopic compositions of the skeletal calcium carbonate paired with the chronology to reconstruct changes in environmental conditions.

Knustson et al. (1972) and Hudson et al. (1976) used X-ray images of stained corals to illustrate the annual high-density bands, from which annual growth rates can be calculated. Application of this extension rate measurement has proven to be extremely helpful in terms of monitoring a range of environmental factors and as indicators for broader climate change. For example, extension rates have been used to evaluate potential effects of fresh water input in the Florida Keys, Gulf of Mexico and China Sea (e.g. Dodge and Lang 1983; Smith et al. 1989; Carriquiry and Horta-Puga 2010; Chen et al. 2011), ocean acidification and (e.g. Cohen and McConnaughey 2003; Lough and Cooper 2011) pollution in the Caribbean (e.g. Dodge 1982; Dodge et al. 1984; Lough and Cooper 2011), and as overall climate monitors in the Gulf of Mexico, the Great Barrier Reef and Pacific Islands (e.g. Buddemeier et al. 1974; Lough and Barnes 1990; Lough 2008). Each of these examples and numerous other studies depend on interpretations of X-ray images of coral skeletal structure paired with measurements of coral extension rates to provide a necessary underlying framework that supports the rest of the study.

For most scleractinian coral studies, once a core of skeletal material is collected from a study site, a rectangular slab is cut from it and an X-ray image is generated to

show variations in its structure. Before this cut is made, the internal structure of the coral core is poorly known. Depending upon the orientation of a core when the slab of skeletal material is cut, the resulting slab is sometimes unusable due to relative corallite growth direction. A "good" coral core slab would contain many individual corallites made by polyps with their growth axes within the plane of the slab; it would show the walls of corallites as long parallel lines that are perpendicular to the high and low density annual growth bands. A "bad" coral core slab would contain individual corallites made by polyps with their growth axes at an angle or, worst-case scenario, perpendicular to the plane of the slab; it would show the walls of corallites as ovals or circles. It should be noted that the apparent extension rate determined from a "good" slab might still not equal the actual extension rate if significant changes in the positions of polyps relative to one another occurred as the coral grew. This methodology has limitations from the unknown alignment of corallites relative to the plane of the image and the effects from the orientation of corallites within the slab, introducing biases that may impact the fundamental extension measurements and the conclusions drawn from them.

The purpose of this thesis research is to better understand and account for factors that affect how accurately coral extension rates can be determined. Coral extension rates determined from both "traditional" slab and computed axial tomography (CT scan) images of the skeletal material in a suite of short *Montastrea faveolata* coral cores from the Flower Garden National Marine Sanctuary. CT scanning is a diagnostic tool initially used for medical purposes, but has since been adapted to other scientific applications, including geosciences (e.g., Bosscher 1993; Ashi 1997; Cnudde et al. 2006; Duchesne et

al. 2009; Saadat et al. 2011). The CT scanning approach allows the internal corallites to be imaged and extension rates to be measured at different orientations without disrupting the core. This non-destructive methodology will enable comparison of extension rates determined several ways: 1) across a single slice or slab X-ray image, 2) between 0.6 mm slice and 8.4mm slab X-ray images, and 3) among slice/slab orientated at varied angles relative to a coral core's longitudinal axis. Additionally, the true three-dimensional extension rate of individual corallites was determined and compared to the extension rate apparent on a two-dimensional slice/slab.

2. BACKGROUND: CORAL SKELETAL STRUCTURE AND MEASUREMENT

Individual coral colonies as well as mollusks, algae, and other organisms form coral reefs. Each individual coral organism is called a polyp; many polyps make up a coral colony (Milliman 1974). The $CaCO_3$ skeletal material deposited behind a growing polyp is called a corallite; by studying the skeletal remains of growth, conclusions can be drawn on changes to the marine environment over time (Vernon 2000a). Colonial hermatypic reef-building hard corals of the Phylum Cnidaria, Class Scleractinia have a symbiotic relationship with photosynthetic algae that live within their tissues. This alga, called zooxanthellae, photosynthesizes and provides the coral with approximately 90% of its needed nutrients while receiving essential nutrients from the individual coral (e.g. Goreau 1959; Goreau and Goreau, 1959; Milliman 1974; Lough 2008). The zooxanthellae also aid in the calcification of hard corals, helping build the structure of the coral colonies (Milliman 1974, Lough 2008). The zooxanthellae are contained within the polyp's endoderm, a double-walled sack within the inner most layer of tissues. The mesoglea is a connective layer separating the endoderm from the outer cell layer, the ectoderm. These tissues are all surrounded by the theca (or the corallite wall) a tube like structure that is the main $CaCO_3$ skeletal component of the coral, Figure 1.

As a polyp begins to grow, the organism "pulls itself up" the ever extending corallite skeletal tube. While growing outward from the base of initial growth, the dissepiment, the polyp cuts itself off from the uninhabited skeletal tube below (Barnes 1970, Cohen and McConnaughey 2003). Each polyp is an individual biological entity

and grows independently of surrounding polyps; they do not follow a "determined" path of growth. A *Montastrea* colony forms through the process of budding, the asexual reproduction of a single polyp (Vernon 2000a).

Within a colony, many individual polyps grow at the same time with only the top millimeters of colony containing the living tissue with the rest of the colony being unoccupied aragonitic skeleton (Vernon 2000a, Cohen and McConnaughey 2003). The length of the corallite contains skeletal plates called septo-costae, radial elements to the skeletal structure. The costae radiate out from the thecal wall and the septum radiate in from the thecal wall (Vernon 2000a). This radiating pattern is what is often seen on coral heads during the day while the polyp is retracted into the coral head (Barnes 1974).

As corals grow, density bands, similar to tree rings, form with the changing seasons (Hudson et al. 1976). *Knutson et al.* (1972) first determined that the high and low density bands occur on an annual cycle by observing elemental concentration changes due to nuclear bomb tests. They showed that generally a couplet of high and low density bands represents a single annual cycle. By cutting a coral core into a slab, the coral can be X-rayed to visually determine the locations of these high and low-density bands. Since high and low density bands form annually, knowing the date at which the coral was sampled can create an age model. High-density bands develop in the late summer and winter low-density bands form during cooler months (Lough and Barnes 1990). Importantly, these annual density bands represent both the extension rate of the coral as well as the calcification (Barnes and Devereux 1988).

a)

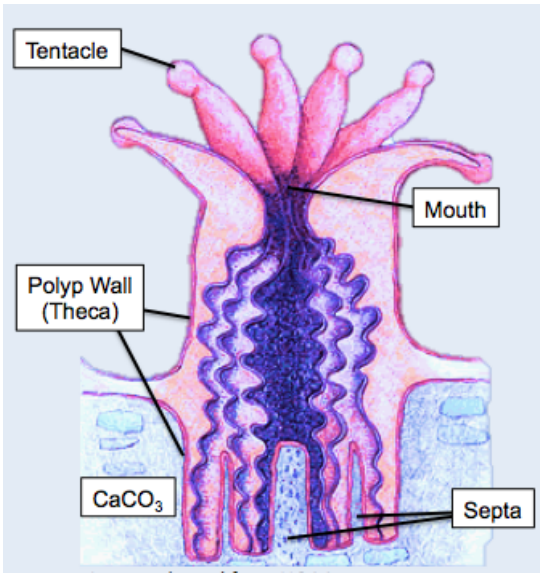

b)

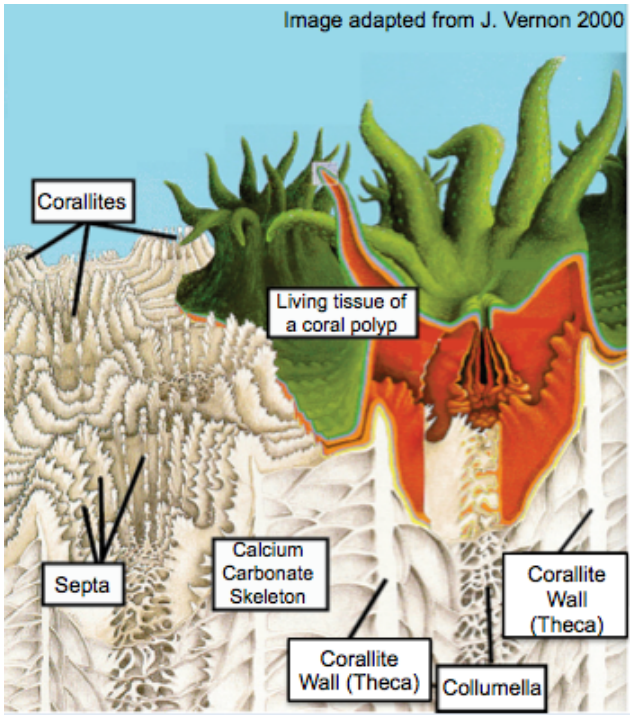

Figure 1: Coral polyp and skeletal make up, a) Coral polyp anatomy, image adapted from NOAA, b) Coral skeleton and polyp anatomy, image adapted from Vernon 2000a.

Conventional extension rates, or the apparent extension rate, are calculated based upon an X-ray of a single slab of a coral core. The angle at which the slab is taken may not be well positioned for calculating the actual extension rate. Ideally, the slab plane should be parallel to the longitudinal axes of the corallites as well as perpendicular to the high-density bands. The downfall to these slabs is that they show only a 2-dimensional view of a 3-dimensional sample, so skewing the apparent extension rate. Conventional growth rates do not take into account the three-dimensional direction of coral growth, but instead the distance between growth bands, which can be distorted based upon the geometry of the polyp growth pattern.

Hounsfield and Cormack developed the computed axial tomography (CT) scanner in the late 1960s and early 1970s to nondestructively view the internal structure of an object in cross-sectional slices (Hounsfield 1973). By using computed tomography scanning (CT scanning), the internal corallites can be observed without cutting into the core. This allows for extension rates to be taken at different digital "slab" orientations within the same core. By using CT technologies, the ideal orientation and angle of the slab to be used for the age model can be determined without cutting the coral core. Additionally, individual polyps can be followed to determine the actual extension rate within a core as well as determine the conventional extension rate. While CT scanning has been used in previous coral studies (Logan and Anderson 1991; Bessat and Buigues 2001; Cantin et al. 2010) it has never been used to follow individual polyp growth paths or to determine the optimal plane for slabbing.

3. STUDY SITE

The Flower Gardens National Marine Sanctuary (FGNMS) is situated in the Gulf of Mexico, approximately 180 km south of the Texas/ Louisiana boarder. This area is made up of dozens of banks along the continental shelf (Rezak et al. 1985). The marine sanctuary contains two banks of interest for this study: East (EFGB) and West (WFGB) Flower Gardens Banks, which are approximately 19 km apart. These banks are made up of two distinct coral reefs that cap salt domes on the continental shelf (Nettleton 1957).

The East and West Flower Garden Banks are just two features among many banks in the northwestern Gulf of Mexico, Figure 2. All of these features are interconnected within a regional ecosystem. The Flower Gardens and surrounding banks are highly affected by the currents of the Gulf of Mexico, specifically the warm waters from the Caribbean and the Gulf Loop, which bring in waters from deeper areas of the Gulf of Mexico. Furthermore, there is discharge from terrestrial inputs, predominantly from the Mississippi watershed (Rezak et al. 1985, Schmahl et al. 2008).

In 1992, the Flower Garden Banks was designated as a National Marine Sanctuary. The reef system is made up of mostly “large boulder shaped” coral colonies with the reef crest depth at approximately 18 m, extending down to depths greater than 42 m. Biodiversity at these locations is spectacular, with a wide range of micro- and macro-organisms. The two most abundant species of coral present at EFGB and WFGB are *Montastraea sp*. and *Diploria strigosa*. Below 42 m, the habitat changes from hard, large boulder shaped corals to an algal sponge habitat and continues to change as depths

increase (Schmahl et al. 2008). We are concerned with those corals in the shallower depths (18-25 m) of the banks.

The *Montastrea* genus of corals is found worldwide and has its earliest fossil record from the Eocene in the Caribbean. We are specifically concerned with the coral species *Montastrea faveolata*, (order Scleractina; subclass Zoantharia) sub taxonomy of *Montastrea annularis*. These corals can be found as massive, yellow-brown dome-shaped colonies with corallite surfaces flush to the surface of the colony. They are found throughout the Gulf of Mexico and Caribbean Sea and are generally the dominant species in lagoons and on the upper reef slopes (Vernon 2000b).

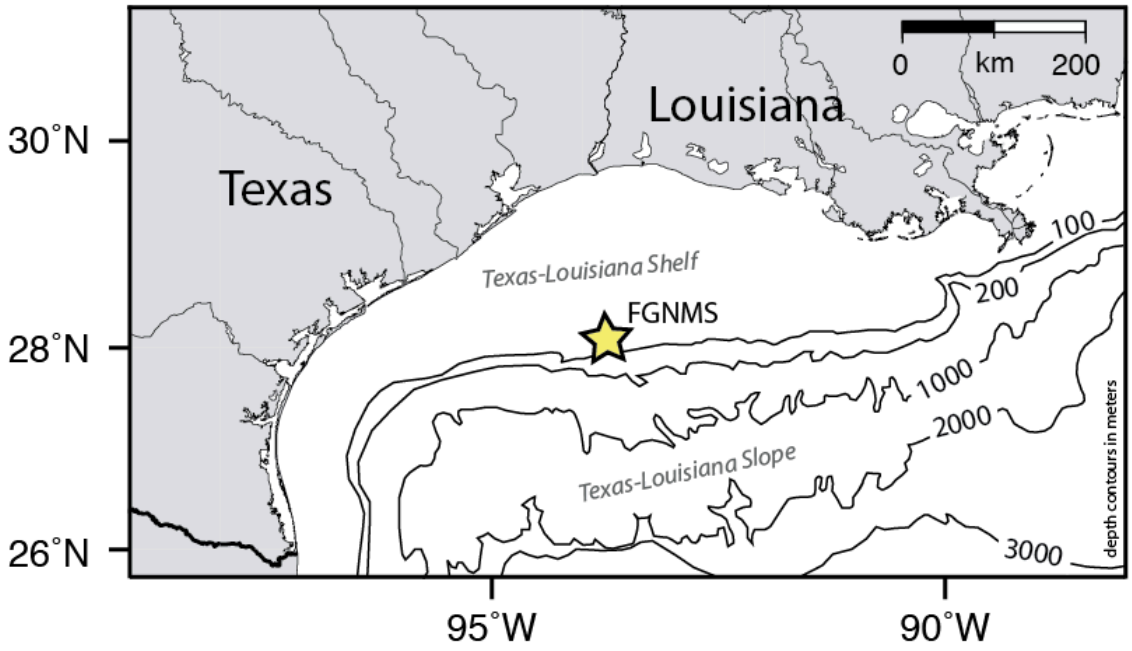

Figure 2: Location map of the Flower Gardens National Marine Sanctuary (FGNMS). Located 180 km from the Texas-Louisiana boarder on the continental shelf, the study area is composed of two banks within the FGNMS, East and West Flower Garden Banks

4. METHODOLOGY

In July 2012, a team of NOAA divers operating from the ship *RV Manta* used an underwater hydraulic drill to collect cores of coral skeletal material at the East and West Flower Garden Banks under permit number FGBNMS-2009-001.

Buoys were moored near the middle of the crests of the two banks (27°54'31.9" N, 93°35'49.0" W and 27°52'30.6" N, 93°48'54.1" W, respectively). A 100 m x 100 m region was identified about each buoy and a core was taken from the central portions of hemispherically-shaped *Montastrea faveolata* corals living at or near the North East (NE), North West (NW), South East (SE) and South West (SW) corners of each region (a detailed description of core sample locations can be found in Appendix II). At two corals, the quality of the initial core recovered was not certain so a replicate core was taken, thus, a total of ten cores of coral skeletal material were collected. These cylindrical cores had a diameter of about 3 cm and lengths that ranged from 5 to 17 cm. The cores were placed in padded, alcohol-filled sections of plastic pipe, and refrigerated to preserve the coral skeletal material and reduce disturbance during storage and transport.

At Texas A&M University, the cores were removed from the alcohol and inspected. The 3-dimensional structure of the coral skeletal material in each core was imaged using a Siemens SOMATOM 40 slice helical CT scanner at the College of Veterinary Medicine and Biomedical Sciences. The longitudinal (also termed z-axis) of each core was aligned parallel to the scanner bed and perpendicular to the center of the rotating X-ray source-detector ring. Beams of X-rays were passed through points in the

core that intersected the plane of the X-ray source-detector ring at angles ranging from 0-360° and their strengths after passing through the core were measured.

Based on these measured values, a matrix of X-ray attenuation coefficients were calculated for a grid of adjacent 0.6×0.6×0.6 mm volumes corresponding to the plane, hereafter termed a "slice" (Hounsfield 1973; Wellington and Vinegar 1987). Small variations of the attenuation coefficient can be significant, so by convention the values for each volume were expressed in the form of CT numbers, also known as Hounsfield units, via the comparison of the X-ray attenuation coefficient of the material (μ) to that of water (μ_w): $CT = (\mu/\mu_w - 1)*1000$ (Hounsfield 1973; Brooks and DiChiro 1976; Wellington and Vinegar 1987). As the core moved through the X-ray source-detector ring, CT numbers for successive slices of coral were computed, resulting in a three-dimensional matrix of CT numbers. A material's tendency to attenuate X-rays by absorption and scattering depends strongly (but not solely) on density (Brooks and DiChiro 1976; Wellington and Vinegar 1987; Boespflug et al. 1995). Changes in CT numbers therefore reflect spatial variations in the bulk density of the coral skeletal material associated with the presence of the coral skeleton's aragonitic structural elements and intervening void spaces. To allow digital images of the coral skeletal material to be created and quantitatively analyzed, the CT values were associated with grayscale values where smaller CT values (lower densities) correspond smaller grayscale values (darker gray) (Brooks and DiChiro 1976; Wellington and Vinegar 1987).

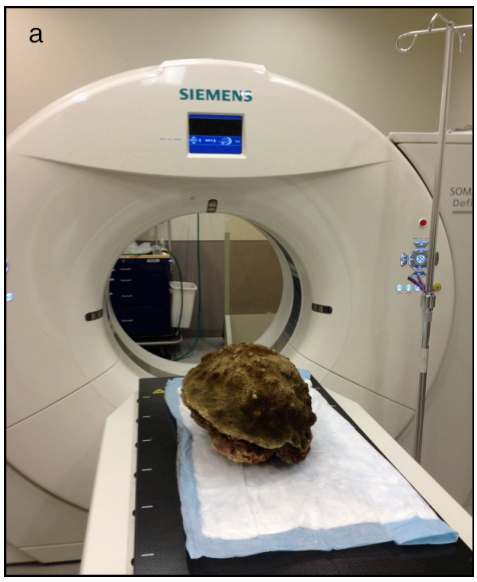

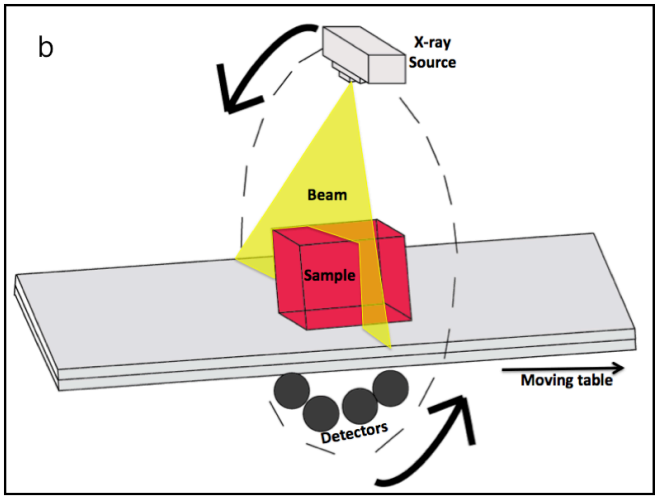

Figure 3: Image and schematic of the CT scanner used for this study, a) Photo of the CT scanner at the College of Veterinary Medicine and Biomedical Sciences at Texas A&M University scanning a coral head, b) Schematic illustration of CT scanner with rotating X-ray source and detectors while scanning a sample.

Given the three-dimensional matrix of CT numbers, it was possible to calculate the CT values and simulate the X-ray images that would correspond to adjacent 0.6 mm thick slices of skeletal material that pass through (or are parallel and very near to) the longitudinal axis the coral core at various orientations relative to horizontal

There were four different slice orientations (0°, 45°, 90°, and 135°) for the WFGB NW, SW, and SE-A cores, while there were three slice orientations (0°, 45°, and 90°) for the other WFGB cores and all of the EFGB cores. Standard DICOM format files of the X-ray images generated by the Siemens CT scanner for each slice were loaded into OsiriX medical image processing software (Rosset et al. 2004). An image like that which would have been a traditional X-ray image from an 8.4 mm thick slab of skeletal material cut from the coral core at each orientation was created by calculating the average pixel grayscale values of 14 adjacent 0.6 mm thick slices simulates this "slab".

Each digital slice and slab X-ray image was examined to identify the couplets of high and low density bands that the coral formed each year (and also occasional high density band is formed in response to a stressful, particularly cold, winter temperatures) (e.g., Knustson et al. 1972; Hudson et al. 1976). Starting at the top of the coral core where the most recently deposited skeletal material was formed; couplets of annual density bands were counted and used to identify the year each was deposited.

The conventional linear extension rate of the coral was measured on each slice and slab X-ray image. TIF format versions of the X-ray images were loaded into the ImageJ software package (Schneider et al. 2012). Three straight transect lines (linear

"region of interests") were drawn to measure the changes of grayscale corresponding to the annual density band couplets, with each transect line following the apparent corallite walls while remaining as perpendicular as possible to the growth bands. To see the locations of each transect across any slice or slab see Appendix III. For each transect, pixel grayscale versus distance was determined and the distance between summertime high-density bands indicates the annual extension rate of the coral for specific time periods.

When the DICOM format images were loaded into OsiriX software, corallites produced by individual coral polyps could be clearly identified in the transverse slices taken perpendicular to the longitudinal z-axis of a core. The extension of individual polyps was traced by following individual corallites across adjacent transverse slices. Annual high-density growth bands show up as waves moving across the core. The x and y coordinates and slice number of an individual corallite was recorded as it passes through each subsequent annual high-density growth band. Given the x- and y-coordinates and the z-coordinate, determined from the slice number and the distance between slices (0.6 mm), the actual extension rate of individual coral polyps was calculated and any potential movement of the polyp across the coral head over time was discovered. At least three individual polyps in each coral core were investigated in this fashion (For a more detailed description of methodology, please see Appendix I).

The determination of conventional linear extension rates along three transects per each slice and slab X-ray image allowed the effects of the following potential factors to be evaluated: 1) variation across a single slice or slab X-ray image, 2) differences

between slice and slab X-ray images, and 3) differences of slab/slice orientation relative to the longitudinal axis of a coral core (i.e., the variation between “good” and “bad” slabs within a single core.

5. RESULTS

Our results are presented through an assemblage of figures and tables. An example of this data reported is presented for WFGB SE-A in Figures 4 and 5 and Tables 1 and 2.

Each core has two sets of figures and three tables. All figures are reported in Appendix III and tables are reported in Appendix IV. The first figure for each core shows the locations of the three transects used for measuring the annual extension rates for the individual 0.6 mm slices at varying orientations 0°, 45°, 90° and, in some, 135°. The second figure shows the digitally created slab at each orientation and the locations of the three transects used for the annual extension measurements. Each slab is the average pixel intensity of 14 single 0.6 mm slices, produced to represent the traditional X-ray image, herein referred to as the slab. For each core there is also a table showing the average measured extension for each set of slice images and the same for each set of slab images. Any blank spots in the table are associated with no measured extension rate for that year at the specific orientation.

Tables 4 and 5 show the average measured actual polyp extension rates across all the cores. EFGB NW does not have an actual polyp extension rate because of *insitu* asexual budding made it impossible to follow single polyps through the core. Due to the lack of a full data set for EFGB NW, it has been excluded from all average growth calculations. All results are presented in centimeters and the estimated time intervals begin in July of 2012 (the month of collection).

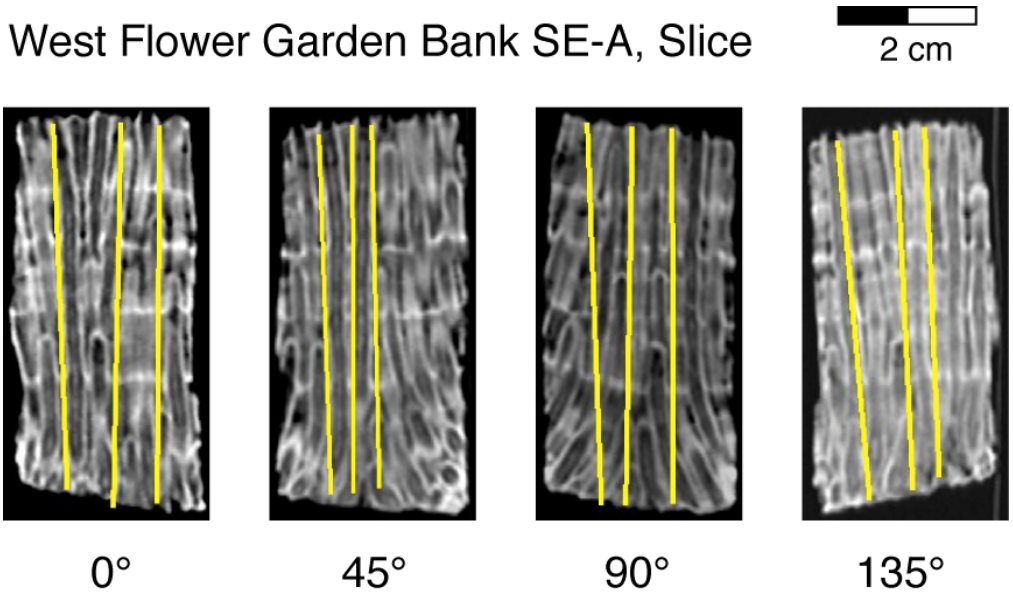

Figure 4: Images of the approximate locations of the three transects (yellow lines) across the 0.6 mm individual slices at orientations 0°, 45°, 90° and 135° of the WFGB SE-A core. See Appendix III for all additional core images.

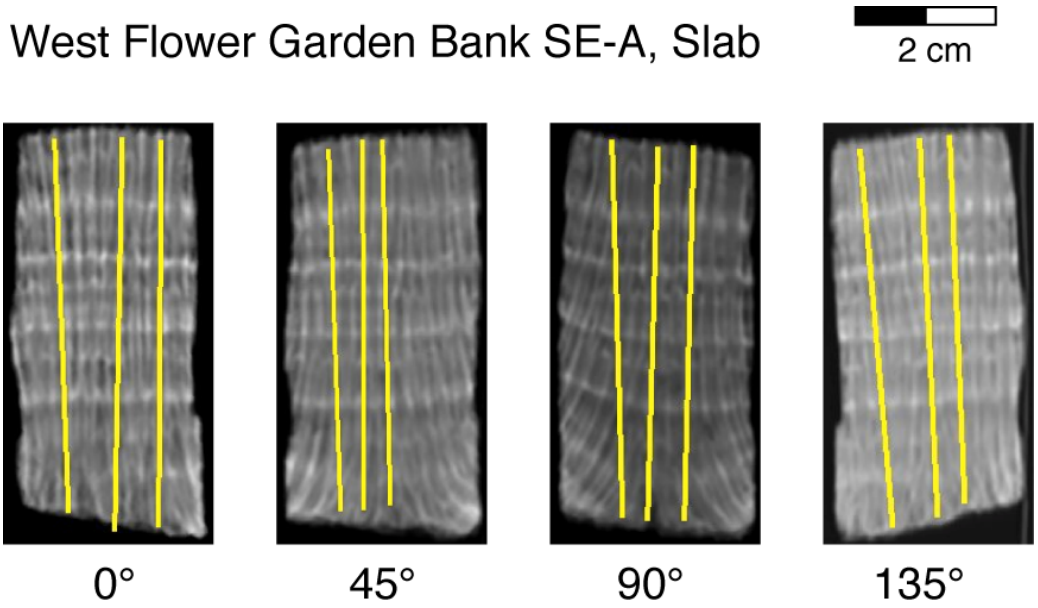

Figure 5: Images of the approximate locations of the three transects (yellow lines) across the digitally created slab at orientations 0°, 45°, 90° and 135° of the WFGB SE-A core. See Appendix III for all additional core images.

Table 1: West Flower Garden Bank southeast-A core average annual extension across the single 0.6mm slice orientations of 0°, 45°, 90° and 135° in mm/year.

Year	Estimated Time Interval	0°	45°	90°	135°
1	2012-2011	6.90	10.96	7.45	9.19
2	2011-2010	9.84	12.03	9.57	8.08
3	2010-2009	9.57	7.29	13.04	9.51
4	2009-2008	10.00	7.94	7.81	10.00
5	2008-2007	11.57	10.43	8.36	10.62

Table 2: West Flower Garden Bank southeast-A core average annual extension across the slab orientations of 0°, 45°, 90° and 135° in mm/year.

Year	Estimated Time Interval	0°	45°	90°	135°
1	2012-2011	8.75	3.79	7.50	9.51
2	2011-2010	7.80	12.32	9.16	8.02
3	2010-2009	9.53	9.59	9.06	9.48
4	2009-2008	9.53	9.95	9.77	9.61
5	2008-2007	10.35	8.58	8.86	7.53

6. DISCUSSION

6.1 Corallite orientation effect on apparent extension rates

It is worthwhile to examine 3D models constructed to illustrate the difference between a “good” and “bad” coral slab orientations. Two factors determine whether a slab is “good” or bad”: the direction of polyp growth and the orientation at which the core is initially taken from the coral head. Figure 6 illustrates how the different orientations of a single core change greatly based on the angle of coral growth within the coral head. In other words, though the core is generally taken perpendicular to the top surface of the coral head, the angle of corallite growth is not always perpendicular to that plane of sampling. As the angle of corallite inclination increases, it can be observed that smaller circles or ovals are seen at changing orientations of slabs. This is important because in “bad” slabs and in some “good” slabs the apparent measured extension rate does not equal the actual extension rate, resulting in inaccuracies between measurements.

It is important to understand how to determine if a slab is “good”, and therefore usable, for accurate measurements. Illustrated in Figure 6, a core with corallite growth axis parallel with the orientation of the slab has the same conventional and actual extension rate, see “Core A”. This orientation would be the optimal condition under which true extension rates should be measured. Conversely, if the corallite growth axis is at an angle to the plane of the slab, see “Core B” and “Core C” at orientations 45° and 90°, the actual extensional rate may be different than the conventionally calculated

extension rate depending on the slab angle taken. This would result in larger extension rate measurements compared to the true extension.

When polyps are inclined and/or the slab is taken at a "bad" angle, the smallest measured extension would be closest to the true extension, see Figure 7a. In these illustrations, each corallite within a core is idealized to be growing at the same angle, this is a simplified illustration since each polyp grows independently they would not follow the same exact alignment. Additionally, when applying trigonometry to attempt to predict the variability within a core based on corallite inclination, a wide range of extension rates are produced. In Figure 7b, an equation was applied to test how high the angle of inclination must be in order to produce irregularity in extension rates greater than that of natural variability. Based on four different actual extension rates, the apparent extension rates were predicted. By observing the resulting graph, it appears that from 0° inclination to approximately 20° inclination, the polyp angle does not have a significant effect on the extension rates. However, angles larger than 40° cause an exponential increase in extension rates.

By determining if a core can produce a "good" or "bad" slab, the following results can be discussed: Transect variability and slice versus slab, Changing orientations, 3D individual polyp extension rates, and East versus West Flower Garden Banks. By comparing all observations, we will determine if there is an optimal way to measure extension rates. In practice for studies that rely upon accurate extension rate measurements, any cut slab with corallites showing ovals or circles is deemed unusable, however in this study all transects are used to show variation within the dataset.

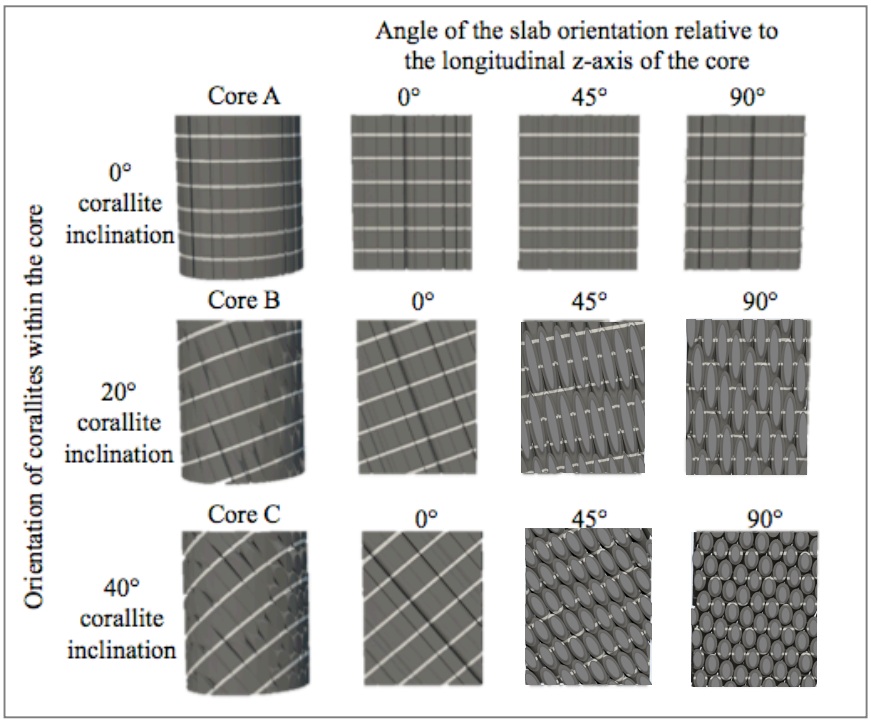

Figure 6: 3D reconstructions of coral cores taken with varying polyp inclinations and the resulting slabs taken at different orientations relative to the longitudinal z-axis of the core. Each Core (A, B & C) has 3 different slab orientations taken from them (0°, 45° and 90°). The increasing polyp angle within each core shows how the slabs change and can be either "good" or "bad" orientations for extension rate analysis. The white bands represent annual high-density growth bands.

a)

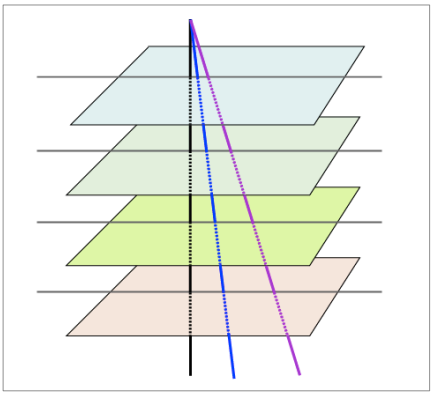

b)

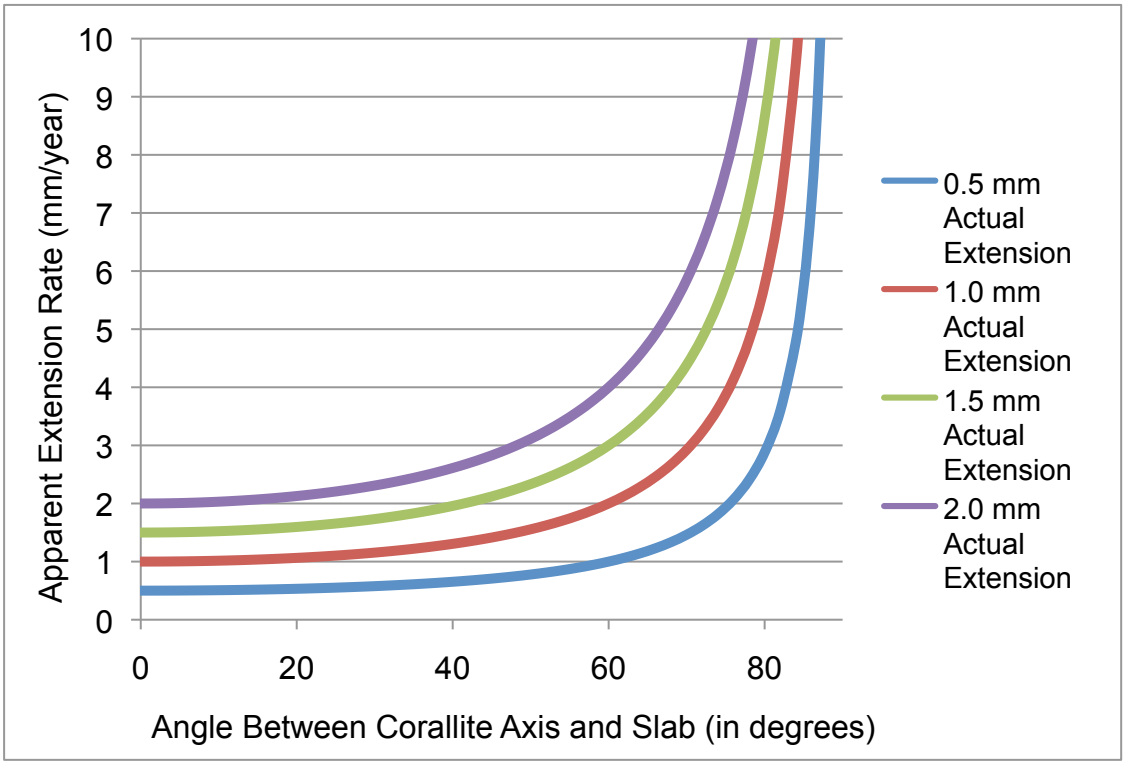

Figure 7: Visual and mathematical models of changing extension rates based on increased inclination. a) Four high-density annual growth bands, showing the variations of measured extension rate. The black line illustrates the true annual extension, blue and purple lines show different potential actual extensions based on increasing polyp inclinations, the black line is always less than the other two, the shortest distance from one high density band to the next is the closest to true extension, b) The results of mathematically modeling for slab inclination based on measured extension rates and the angle of inclination.

6.2 Transect variability and slab versus slice

The next step in this study is to compare extension rates measured on a single slice and a slab of the same core per orientation. Based on visual assessment of the data, extension rates determined from the digitally constructed slab results of any given orientation of a core are muted compared to the 0.6 mm slice transects, see Figure 8. Depending on the location of a transect line in a single slice, it is possible to have a transect line go through a corallites collumella (refer to Figure 1b), where the skeletal material is extremely thin or void. A transect line passing through this potentially void space could miss a high-density band, as in Figure 9. However, when using the average pixel intensity slabs, many of these "missed" bands are accounted for. Single slices have a greater dynamic range of pixel values due to abrupt density changes. Conversely, a slab is the average pixel intensity of 14 slices, seldom having any void space present after combining the slices together. Additionally, on a single 0.6 mm slice, stress bands are expressed more (more easily seen) and can skew the data by being interpreted as a high-density annual band. Where as on the slab, these stress bands can be filtered out more easily, through averaging the pixel intensities. Either method can still resolve where the high-density bands are located but using the average pixel intensity slab makes the trend visually clearer, reducing the noise of increased variability within a slice.

In practice, when measuring extension rates the transect lines would be placed at a location where the high-density bands can be distinguished the best, parallel to the corallite wall. The position of the transect lines would want to cover the greatest density

differences while remaining perpendicular to the high-density bands. For this study, the location of the transect lines is standardized to test the sensitivity of slice to slab, not to include a visual inspection bias. This is completed by orientating three transects along a given slice at the locations where high-density bands can be best observed and using the same three transect line spatial locations across the associated slab.

The variability between measurements of individual transects is tested. The percent difference of extension rates is calculated for the three transects across every measured slice and/or slab. Variations in extension rates of slabs for individual years measures between 1.5% and 88% in WFGB and 0% and 72% in EFGB. The difference in transects across single years can be large and attributed to variations across individual years on a single slab. However, the average percent difference between transects across all the cores in EFGB is 17% and in WFGB 18%, indicating that the natural variability of the coral growth may cause these discrepancies instead of corallite orientation.

In all cores, when comparing a slice to a slab, the standard deviation between the annual extension rates measurements of all transects is calculated. The standard deviations are being used as a relative measure of precision between slice and accompanying slab. Based on the three linear transects drawn across a slice or slab, the smaller the standard deviation between the three associated transects, the more precise the annual extension rate. At EFGB, the slab measurements, on average, are 63.8% more precise than the slice annual extension rate measurements, see Table 3. At WFGB, the slab annual extension rates are, on average, 69.5% more precise that the slice measurements. These are calculated without excluding bad orientations (to be discussed

in section ‘Changing orientations’). For all cores but WFGB NW, the slab extension rates are more precise than the 0.6 mm slices. WFGB NW has standard deviations between the slice and slab transects that are almost equal, with differences between standard deviations being as small as 0.23 mm.

Figure 10 shows a comparison of all of the annual extension rates obtained from the slab versus the slices. A strong positive correlation between the two data sets, R^2=0.67, exists. While the correlation is strong, the outliers generally fall to the right of the overall trend, indicating a higher annual extension rate in the slices rather than the slabs. This is due to transect lines encountering the void space within corallites, missing the high-density bands and calculating the extension from two years as a single year’s extension. The slabs reduce this problem by averaging the pixel intensities, removing the chance of encountering void, or very low-density, regions.

Consistent with the strong correlation, a comparison of all slice and slab annual extension rates reveals that a significant difference does not exist, with one exception: WFGB NE, 0°. Using a paired T-test, the null hypothesis, H_o: there is no difference between the slice and slab, is accepted since the *p*-value >0.05. Further inspection of the WFGB NE 0° slice versus slab (p = 0.052), shows that the slice had multiple high-density bands missed within each transect, skewing the results.

With this study, the lack of statistical significance (excluding WFGB NE, 0°) verifies that either the slice or slab can be used to calculate average annual extension. However, it is important to pair the slice or slab with a visual inspection to keep the measured extension rates as precise and accurate as possible. It is important to take a

holistic approach when calculating annual average extension rates, using all the evidence and technologies available to make the best measurement possible. We suggest that the slab is used in future studies, reducing the variability introduced from missed high-density bands.

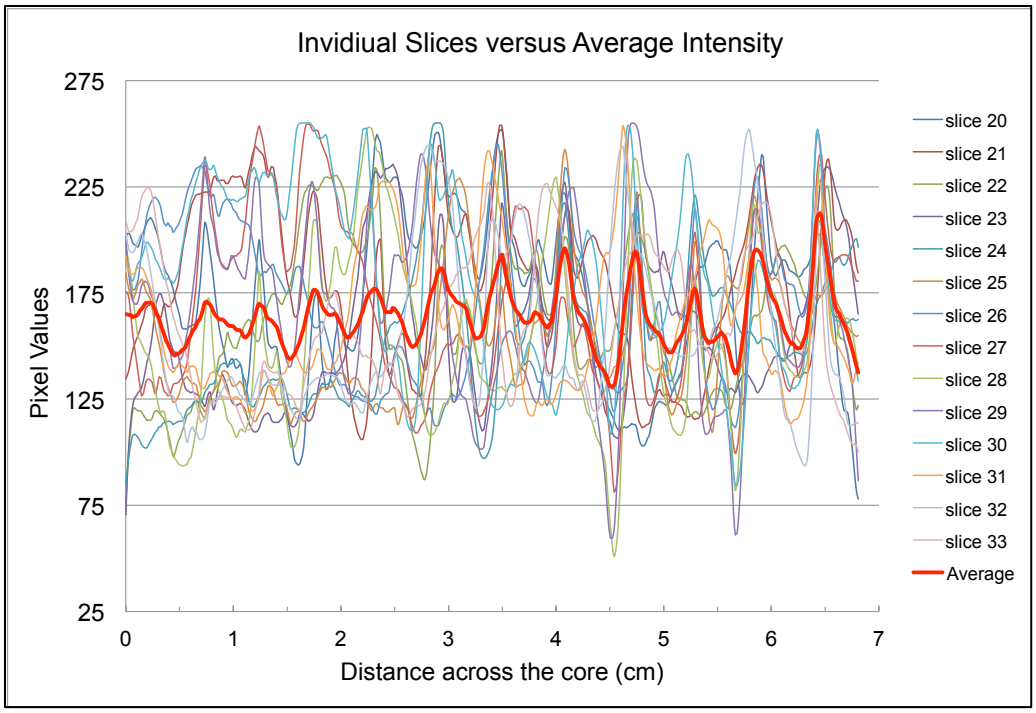

Figure 8: Variability between 0.6mm slices and the associated slab. Using core EFGB SE 0°, a single transect line was drawn across the length of the core. A profile of pixel values along the length of the transect line was taken at each slice from 20 to 33 to show the variability between slices. Additionally, the average intensity was taken from slices 20-33 to create the "Average" or slab for the same transect.

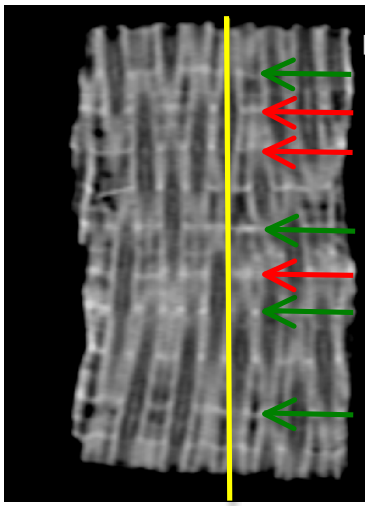

Figure 9: A CT image of a 0.6 mm slice of a coral core showing missed high-density bands. The location of the yellow transect line illustrates how, in a single slice, multiple high-density growth bands may be missed. The red arrows point toward missed high-density bands and the green arrows point to where some high-density bands would be measured.

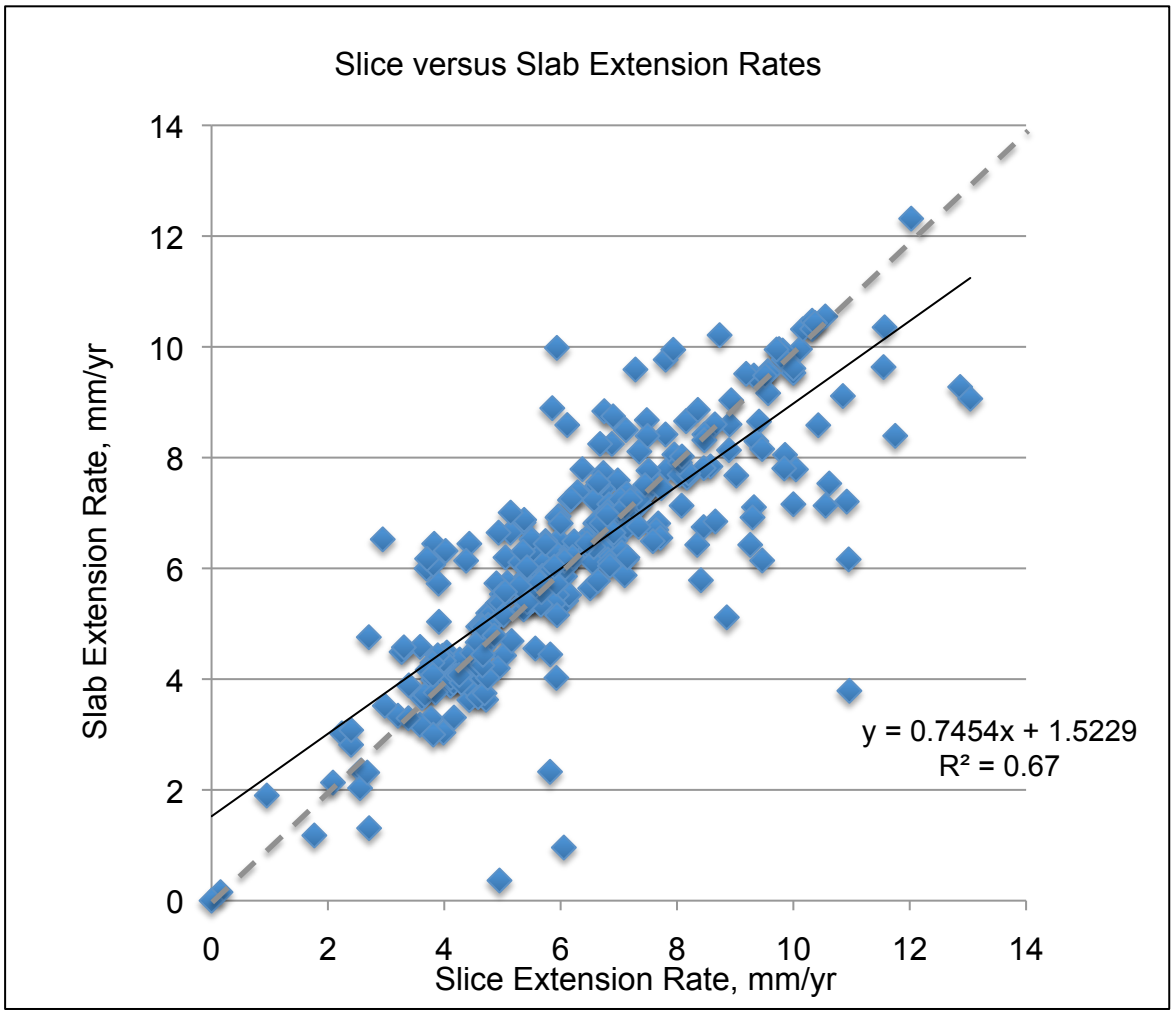

Figure 10: Comparison of slice versus slab annual extension rate measurements. This illustrates the correlation between the slice and slab data set from the same transect line location. The dashed line represents a 1:1 relationship; the data presented is skewed slightly to the right.

Table 3: Based on the standard deviation of annual extension rates, the proportion of times when the slab is more precise than the slice. Note: EFGB NW thrown out of all calculations due to *in situ* budding and the inability to follow individual polyps through the length of the core

CORE	% That Slab is more precise	CORE	% That Slab is more precise
EFGB NE	54.5	WFGB NE	63.6
EFGB SE	69.2	WFGB NW	43.8
EFGB SW top	60.0	WFGB SW-A	80.0
EFGB SW bottom	71.4	WFGB SE-A	60.0
		WFGB SE-B	100.0
Average	63.8	Average	69.5

6.3 Changing orientations

Another concern when measuring annual extension rates within a coral core is the variability present within the core based upon the orientation of the slab being measured. With the application of CT scanning technology, we aim to show the potential extension rate inconsistencies within cores based on digitally changing the slab orientations for each core. The cores were sliced at three or four different orientations relative to the initial position of the core: 0°, 45°, 90°, and, sometimes, 135°. The slab is deemed more precise than a single slice (even though there are no significant differences, as discussed previously); therefore a comparison of orientations was completed using slab annual extension rates of the nine usable cores.

Simple visual inspection of an orientation can sometimes qualitatively determine if it is a "good" or "bad" slab, and therefore suitable for making extension rate measurements. However, we aim to quantify the variability within a core so all orientations created are used. Corallite orientation can cause discrepancies in annual extension rates. For example budding as seen in core EFGB NW, see Figure 8, the corallites are very hard to follow regardless of the orientations taken due to *in situ* asexual reproduction. Additionally the orientation of the slab may cause differences, for example the slice orientations of EFGB SW core, see Figure 9. In practice, visual inspection would determine the EFGB SW 0° and 45° slice orientations to be "bad" slabs and therefore unusable for extension rate analysis (refer back to Figure 6). However, the 0° and 45° slice orientations are used for the purpose of this study.

Since each orientation is relative to the initial position of the core, comparison of specific orientations between different cores cannot be made. In any given core, the extension rates between orientations are highly variable; some annual extension rates obtained have a low standard deviation, 8.4±0.055 mm (2011-2010 WFGB SE-B) and some a high standard deviation 5.37±2.78 mm (2012-2011, EFGB NE). See Appendix IV for the extension rate variability for all cores.

In order to quantify and compare the extension rates from different slab orientations, the significance between orientations of each core is tested in each of the nine cores. Seven of the cores have no significant difference between the measured extension rates among orientations within a single core; however, it is worth noting that several slab orientations are nevertheless considered "bad" orientations based on previous discussion. Two exceptions exist: WFGB NE and WFGB SW-A. WFGB NE shows a statistical difference ($p = 0.0134$) between orientations, rejecting the null hypothesis: H_0 = the changing orientations have the same extension rates. WFGB SW-A shows a marginal significance ($p = 0.08$) between orientations.

One downfall to the presented statistical results is that these tests account for the entire time interval of each core. While the comparison of all annual extension rates across the length of the core may not be significantly different at varied orientations, it does not account for individual years. It may be that some individual years are drastically different between each orientation, for example EFGB NE year 2012-2011 has an annual extension rate of 5.37 mm with a standard deviation of 2.78 mm (i.e., about 52% standard deviation). While quantifying the difference between orientations, it

is important to consider the individual years as well as the complete time interval the core covers. Combining statistical tests on extension rates, visual inspection, and annual data analysis will result in the most accurate results.

Since the orientations are relative to the positioning of the core while being initially CT scanned, the resulting slabs and slices may not be along the most optimum planes. Taking further intervals of angled orientations (i.e. maybe every 10 degrees) would be more likely to capture the plane of maximum growth axis. Overall, the orientation of the slab does not make a significant difference within this specific data set across the cores total time interval. However, all of these cores are short and have fairly parallel corallite inclination (due to a good collection method) and therefore are a good series of cores for climate monitoring studies. Each annual extension rate should be carefully considered separately from the statistical analysis. Future studies may not revel the same result due to more variation between orientations, collection method, core length, corallite inclination, etc.

Figure 11: EFGB NW core slice showing the beginning stages of polyp budding in the plane of interest. The red arrows indicate the area of budding.

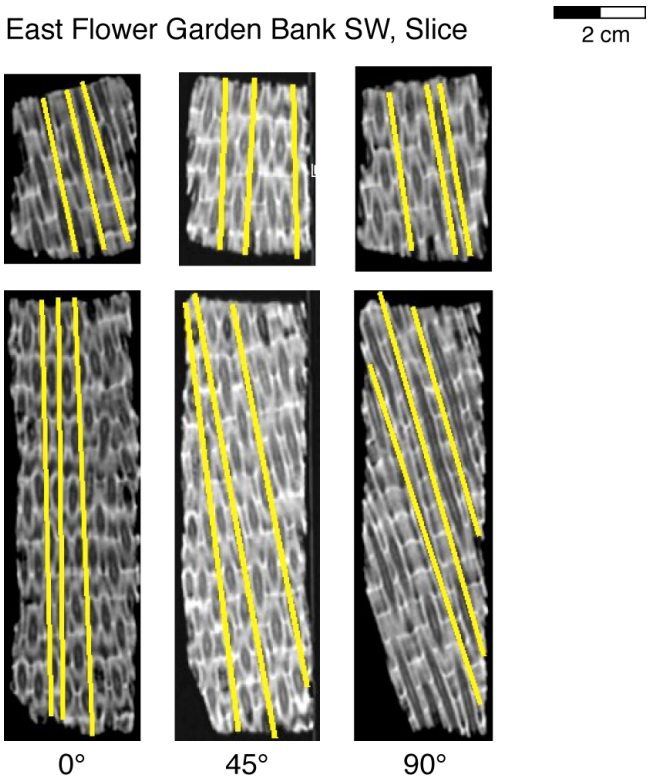

Figure 12: East Flower Garden Bank- SW core slices. Due to the relative orientation of the polyp growth axes, the 0° and 45° orientations would be categorized as unusable based on visual inspection.

6.4 3D individual polyp extension rates

A unique aspect of our work is the ability to compare apparent extension rates measured in planes (i.e. the shortest distance between high-density annual growth bands) with the actual extension rate of individual polyps through a core. As the coral colony grows, the individual corallites do not follow a single direction of growth. Instead, they shift in the x, y, and z direction independently of each other, see Figure 13. By using the transverse cross sectional view produced by the CT scanner, individual polyps are followed along the axis of polyp growth to illustrate their movement within a core. It is this discrete movement of the polyp that may cause a discrepancy between the calculated conventional extension rates and the actual extension rate of a corallite. It is conceivable that if a polyp is oriented at an angle instead of perpendicular to the high-density growth bands, there may be a significant difference between conventional and actual extension. The new methodologies we developed allow for this difference between the conventional and actual extension to be quantified.

Summing the individual x-, y-, and z- spatial components from each annual high-density growth band to the next determined the extension of individual polyps. Three polyps are measured through the length of a single core; each of these extension rate calculations is summarized in Tables 4 and 5. The year of sampling, 2012-2011, is excluded from all actual polyp extension rate measurements due to an incomplete year of coral calcification. The highest standard deviation of extension rates between polyps of the same core is 7.8±2.25 mm, year 2010-2009 in core WFGB SE-B; the lowest standard deviation is 3.62±0.0036 mm, 2009-2008 in core WFGB NW.

It is expected that conventional extension rates are always smaller than the individual polyp extension rate, refer back to Figure 7. However, there are two instances when the actual extension may be less than the conventional: 1) the conventional extension is not measured correctly and therefore the apparent extension is not the true extension and 2) the high-density growth bands are not deposited uniformly and/or perfectly parallel to each other, see Figure 14. Additionally, when observing growth bands in a sequence of transverse (cross-sectional) images in rapid succession, the high-density growth bands often come into view as "waves" moving across the cross sectional view of the core. The direction and rate of the apparent movement of the annual high-density growth band laterally across the core varies based on the changing orientation of the high-density growth planes in the coral. The relative differences are independent of the initial placement in the CT scanner and of the core to coral-head orientation.

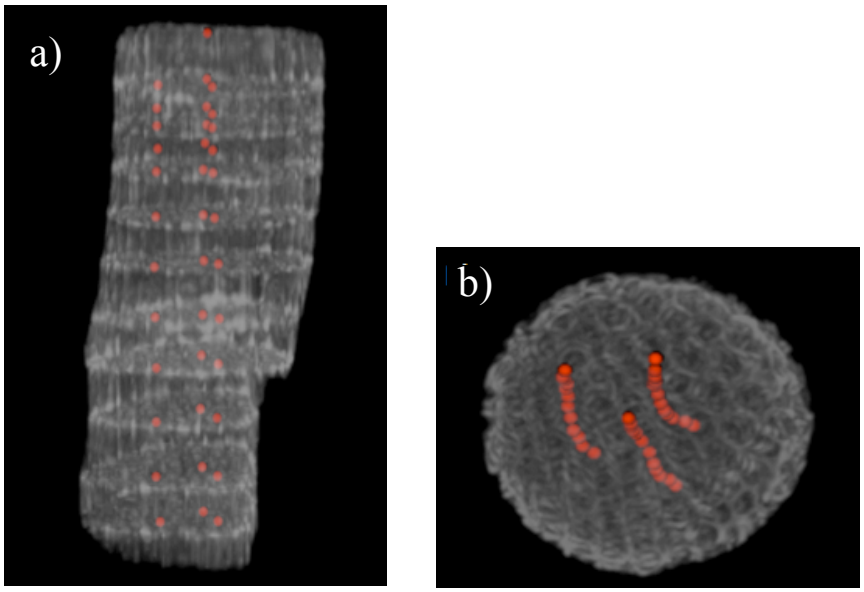

Figure 13: A 3D reconstruction of core West Flower Garden Bank SW-A. a) The high-density bands shown as white planes across the horizontal of the core and the red dots mark the centers of three polyps as they grow upward through the core encountering each high-density band. b) West Flower Garden Bank SW-A core viewed along the longitudinal z-axis of the core, showing the spatial movement of the three polyps in the x- and y- direction along the length of the core.

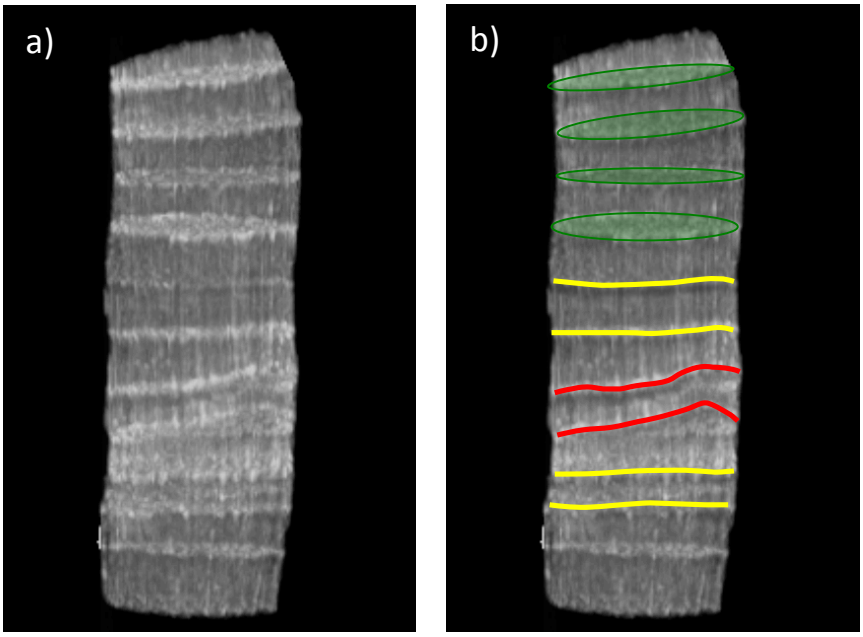

Figure 14: A 3D reconstruction of core EFGB NE showing the uneven deposition of high-density growth bands. a) Image showing the core prior to highlighting the depositional changes. (b) 3D reconstruction of core EFGB NE with highlighted high-density bands. Highlighted high-density growth bands that are evenly deposited are in yellow; in red are two annual growth bands that were not deposited evenly, skewing the extension rate measurements laterally across those specific years. In green, the plane of the high-density growth band has been shifted, also altering potential extension rate measurements.

Table 4: East Flower Garden Bank actual polyp annual extension rate in mm/year

Year	Estimated Time Interval	EFGB NE	EFGB SE	EFGB SW
1	2012-2011	6.42	4.63	5.87
2	2011-2010	6.85	5.01	6.24
3	2010-2009	5.00	5.63	7.14
4	2009-2008	6.67	5.65	7.83
5	2008-2007	8.66	5.87	7.28
6	2007-2006	8.87	5.71	7.05
7	2006-2005	7.69	6.57	7.15
8	2005-2004	7.91	5.93	7.22
9	2004-2003	7.50	5.16	6.71
10	2003-2002	7.49	6.20	6.43
11	2002-2001		6.42	7.23
12	2001-2000		6.48	7.33
13	2000-1999			7.31
14	1999-1998			6.98
15	1998-1997			6.47
16	1997-1996			6.43
17	1996-1995			6.47
18	1995-1994			6.02
19	1994-1993			7.96

Table 5: West Flower Garden Bank actual polyp annual extension rate in mm/year

Year	Estimated Time Interval	WFGB NE	WFGB NW	W SW-A	W SE-A	W SE-B
1	2012-2011	4.90		4.92		
2	2011-2010	5.60	4.03	4.43	8.07	8.81
3	2010-2009	5.58	4.44	2.84	9.45	9.61
4	2009-2008	6.20	2.86	2.57	9.62	8.01
5	2008-2007	7.75	3.62	6.05	12.37	8.73
6	2007-2006	5.54	4.84	6.28		9.74
7	2006-2005	6.17	4.25	7.06		10.38
8	2005-2004	7.18	4.22	6.07		
9	2004-2003	6.89	4.22	7.23		
10	2003-2002	7.51	4.22	7.67		
11	2002-2001	9.16	6.05	6.07		
12	2001-2000		5.86			
13	2000-1999		3.87			
14	1999-1998		3.67			
15	1998-1997		4.45			

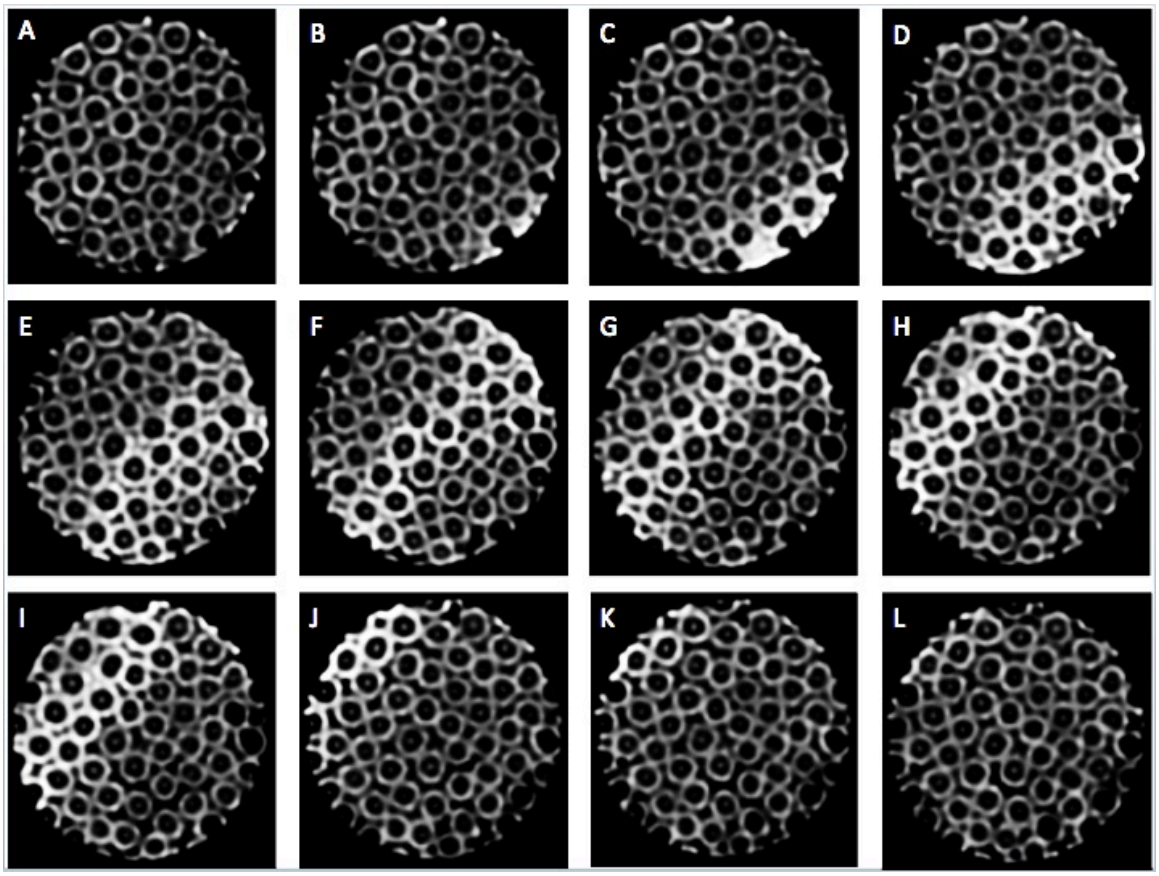

Figure 15 (A-L): Core East Flower Garden Bank NE time series. The images of the core show a high-density annual growth band (brighter sections) moving across the core, bottom right to upper left, as a wave through the transverse cross sectional view. A) 0.6mm slice 50, B) 0.6mm slice 51, C) 0.6mm slice 52, D) 0.6mm slice 53, E) 0.6mm slice 54, F) 0.6mm slice 55, G) 0.6mm slice 56, H) 0.6mm slice 57, I) 0.6mm slice 58, J) 0.6mm slice 59, K) 0.6mm slice 60, and L) 0.6mm slice 61.

Figure 16 shows the individual polyp extension rate versus the conventionally determined extension rate of each core. The conventional extension rate used for each core is determined by the slab orientation with the smallest average annual extension; refer back to Figure 7. The results show a correlation between the two methodologies, $R^2 = 0.57$.

There is no obvious statistical difference between the measured actual polyp extension rate and the apparent slab extension rate at any given orientation within a core. All paired t-tests comparing each orientation with the actual extension rate and the average of all slab extension rates with the actual polyp extension rate result in p-values > 0.05. There is a marginal significance between two orientations and the actual polyp extension in WFGB SW-A, 0° and 90° ($p = 0.12$ and $p = 0.13$, respectively) and in EFGB SE, average of all orientations compared to actual polyp extension ($p = 0.15$). However, these results are not enough to draw significant conclusions against the conventional method of measuring extension rates. As with the comparison between orientations of the same core, the statistics compare the extension rates across the entire time interval of a given core. Even though the statistics show no significance, in order to obtain the most information from a core possible, the orientation and 3D movement of individual polyps should be considered over two time scales: the entire interval contained within the core and on an annual basis.

Measuring the individual polyp extension rate of a coral is a dependable way to ensure that orientation doesn't interfere with calculated extension rates; removing the concern that a slab may be at "good" or "bad" orientation. It also ensures that the measurement takes into account the 3D movement of the coral polyp instead of just calculating the apparent extension rate. Additionally, it is important to note that the individual polyps followed are not necessarily the same positioning as the three transects used for conventional measurements. This may cause discrepancies in extension rates due to high-density growth band deposition, causing extension rates to appear different.

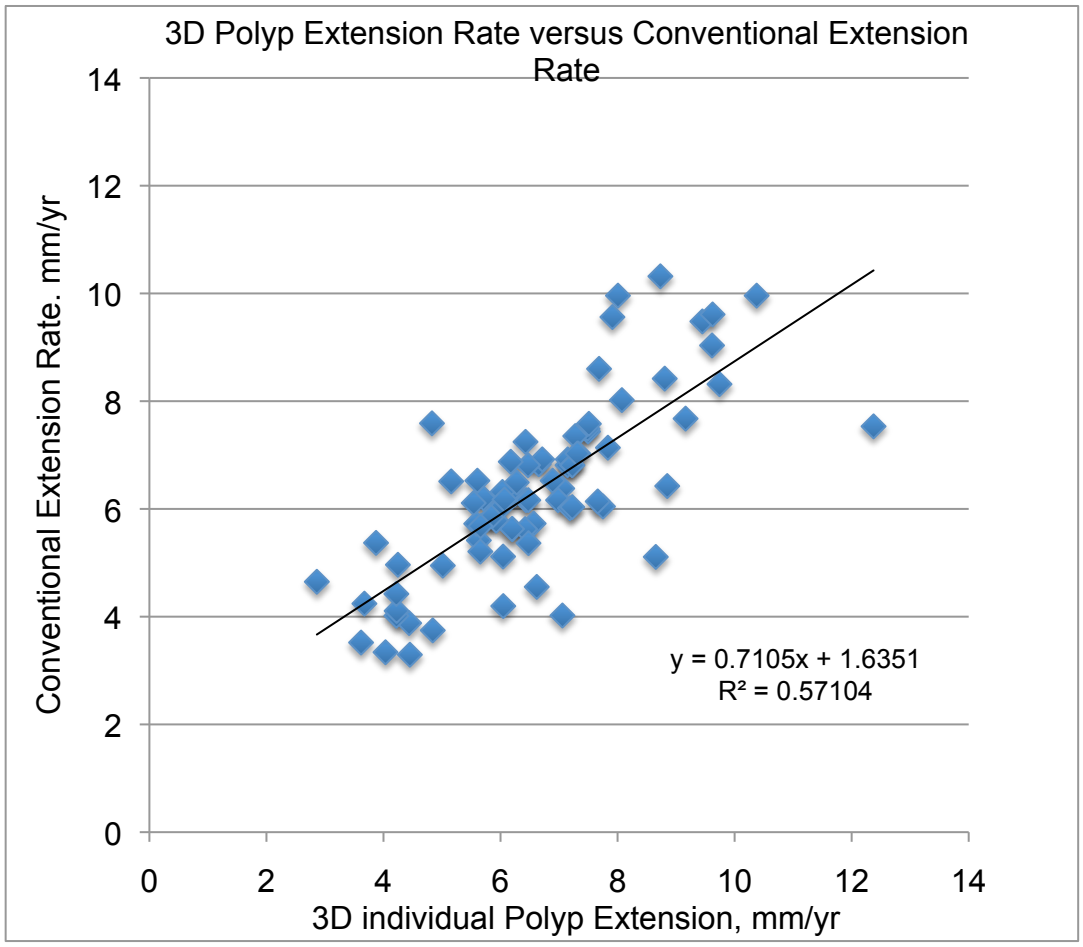

Figure 16: Comparison plot between the conventional extension rate methodology and the actual polyp extension rate methodology, using both EFGB and WFGB. The positive correlation has a $R^2 = 0.57$.

6.5 East versus West Flower Garden Banks

The cores we use for this study show clear differences occurring between the East and West Flower Garden Banks. Since cores were collected from the crests of both reef formations, the extension rate measurements from each bank is used as a measure of biological response to different physical conditions. The two banks have reef crests in about an 18 m water depth but are approximately 19 km apart, introducing potentially different environmental characteristics. Using the average extension rates at each bank allows for a quantitative biological comparison between East and West Flower Garden Banks. The lowest average annual conventional measured extension rate for each core is used to represent the closest to true extension measurement, excluding the first year. Figure 17 shows the relationship between the three cores at EFGB and five cores at WFGB. Interestingly, the EFGB cores have a more similar extension rate over the time interval than WFGB. Using these conventional extension rates, the average extension rates for each bank are listed in Table 6. Cores were collected in water depths between 18 and 22 m (see Appendix II). No apparent correlation exists between average annual extension rate and the water depth where the corals lived. Perhaps there is another factor that causes the distinct change in extension rates between the cores, i.e. water temperature, food availability, surrounding organisms and habitat, pH, current locations, predation, etc.

Additional attention should be paid to the sample collection process. Extension rates can change based upon where on the surface of the coral head the core is taken. For

this study, divers did attempt to collect these cores from a central location within the coral heads, but slight variations could introduce an unwanted bias.

6.6 Previous studies

By comparing the measured extension rates of coral cores from the same area of interest, Wagner *et al*. (2009) and Miner *et al*. (2013), the averages of this study are on the low end of the range of previously measured annual extension rates. The work by Wagner *et al.* extends back until the late 1700's and used the traditional X-ray slab methodology for cores in not only the Flower Gardens, but also from Veracruz Mexico. Miner *et al*. also used conventional methodology for annual extension and has annual extension rates until the mid 1800's. Neither study looked at individual polyp extension, due to the lack of CT technologies. However, both studies allow for an East versus West Bank comparison on a longer time interval. The higher extension rates found in previous studies may be due to measuring the apparent extension rate rather than the actual extension rates of the corals. While the measured extension for the present study is not unpredicted, they do appear to have, on average, low annual extension by comparison. This difference in extension rates may, perhaps, be due to the inclusion of individual polyp extension rate measurements.

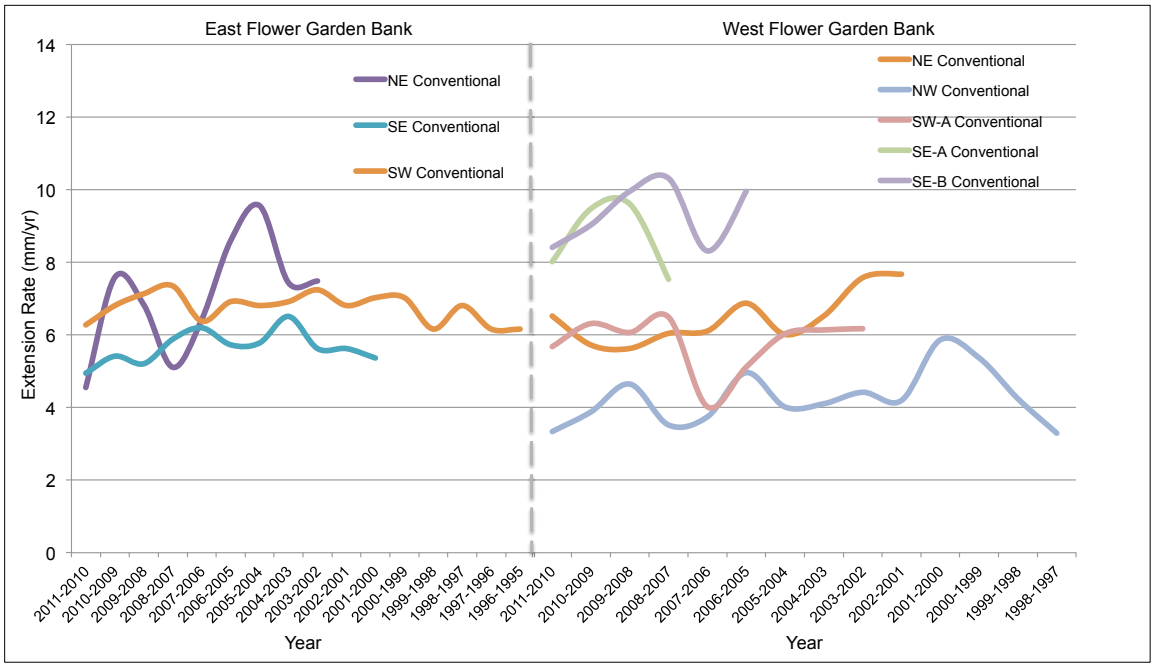

Figure 17: The conventional annual extension rates (mm/year) for each core at East and West Flower Garden Banks over the time period from 1995-2012, excluding 2012-2011.

Table 6: Average annual extension rates at East and West Flower Garden Banks (mm/year). These extension rates were calculated by averaging the orientation with the smallest average annual extension rate within each core for each bank.

Year	EFGB Average	WFGB Average
2012-2011	---	---
2011-2010	5.26	6.4
2010-2009	6.61	6.89
2009-2008	6.39	7.18
2008-2007	6.12	6.78
2007-2006	6.33	4.44
2006-2005	7.08	5.38
2005-2004	7.38	5.35
2004-2003	6.96	5.59
2003-2002	6.79	6.06
2002-2001	6.22	5.94
2001-2000	6.2	5.87
2000-1999	7.03	5.37
1999-1998	6.16	4.24
1998-1997	6.81	3.29
1997-1996	6.16	
1996-1995	6.16	

6.7 Supplementary considerations

Several additional considerations must be made in relation to the results presented for this project. While the methodology works for the cores collected, it maybe difficult in longer timescale studies, such as paleoclimate studies, since the cores are generally much longer in length. Often, long cores (over 1 meter) are used in climate studies, allowing for direction of corallites to change drastically. In the cores we used, polyps generally maintained a uniform direction of growth (excluding core EFGB-NW), but these cores are never more than 17 cm long. Other studies may encounter problems when the cores are a greater length, allowing for more variability. In these cases, CT scanning is highly advisable to observe polyp directional growth and to see if any bioturbation has occurred, potentially throwing off extension rate measurements.

Variability within the data sets should also be noted. While the methodologies ensure the same procedures are used with each core, uncertainties still exist. When initially CT scanning the cores, the initial position is arbitrary. Even though the core is then scanned at either 3 or 4 other angles, the best plane of sampling (corallites running parallel longitudinally, perpendicular to the high-density bands) may be missed. Also, the cores were all taken within the same month; however there may have still been irregularity with the core collection.

7. SUMMARY AND CONCLUSIONS

Because many different types of scientific research and biological/environmental monitoring activities rely upon annual coral extension rate values, it is important to understand the level of accuracy and limitations associated with various methodologies for measuring extension rates and to develop the most accurate procedure possible. We use CT imaging of *M. faveolata* corals to assess factors involved with the conventional approach of measuring extension rates from planar images of coralline skeletal material equivalent to either a 0.6 mm slice or the 8.4 mm thick slabs (average of fourteen adjacent slice images). Four main factors are considered: the orientation of corallites relative to the planar image (i.e., "good" versus "bad" slice/slab), variations of extension rates determined from three separate linear transects across a slice or slab, differences of extension rates determined from corresponding slices and slabs, and differences between various orientations of the slices/slabs relative to the axis of a each core. Additionally, the CT method enables individual corallites to be followed through each core, allowing the direct quantitative comparison of values determined from the conventional planar approach and the actual growth of individual polyps in three dimensions.

For extension rates determined from the three transects across any planar image, statistics indicate no significant difference over the entire multi-year time interval examined in each of the cores. However, for specific years large variations in measured extension rates occur, primarily because of either missed high-density bands in the 0.6 mm slices, or non-uniform distances between adjacent annual high-density bands. Therefore we suggest that when using the conventional method of measuring coral

extension rates, extension rates should be determined from slab images of skeletal material (rather than slices) and average extension rates should be determined from several transect lines across a slab.

Little statistical difference exists between extension values obtained from slab images taken at different orientations relative to the longitudinal axis of most cores examined. This result indicates that the longitudinal axes of these short cores were taken essentially perpendicular to the surface of the coral head, which is the desired practice for the collection of cores for either scientific research or biological/environmental monitoring purposes. Under this circumstance, the conventional approach for measuring coral linear extension rates – obtaining an X-ray image of a uniformly thick slab of skeletal material cut from a coral core – yields accurate results without significant methodological bias.

It is worth noting that while planar image orientation is not a significant factor in this study, it may be for others. Specifically, if cores are taken with less care, or if cores are longer, such as typically is the case for paleoclimate studies, it is likely that the direction of polyp growth will not always align with the core's longitudinal axis. Using CT technology to image the internal structure of long cores allows for the optimum plane of polyp growth axis to be identified and accurate conventional extension rates to be measured. It is also advantageous for choosing where to cut a given section of a long coral core to expose the inner surface of the skeletal material for geochemical sampling.

In addition to facilitating an examination of factors that effect linear extension rate measurements determined from planar images of coral skeletal material, the CT

approach makes it possible for the growth of individual polyps to be investigated. A method is developed for using the three-dimensional volume of CT data to calculate the distance individual corallites extended along their axes during annual growth increments. For any individual coral core, statistics indicate no significant difference between conventional (planar) and actual (3D) extension rates over the entire multi-year time interval examined in each core. Nevertheless, there are differences between extension rates determined for individual annual growth increments. Other than the fact that the conventional and actual extension rate measurements are not made at exactly the same location in the coral core, at least two possible reasons for such differences exit: there may be a non-zero angle between the longitudinal axis of a core and the planar image (conventional > actual) and translation of the polyp locations may occur relative to surface of the coral head as they grow (conventional < actual).

Results presented here indicate linear extension rates determined using the conventional and individual polyp approaches are consistent, so the use of either approach would be appropriate as long as a qualitative assessment of corallite orientation is made. CT imaging has the advantage of non-destructively imaging the internal skeletal structure of the core, although it is more expensive.

The application of CT imaging to follow the three-dimensional growth of individual polyps through time opens up new possibilities for better understanding the biological development of coral skeletal structure. We suggest at least two directions for future research. A practical contribution will be to develop a correction factor to account for the difference between the apparent and actual extension rates of polyps growing at

oblique angles relative to the longitudinal axis of a coral core. Also, insight into the fundamental way coral colonies develop can be obtained by investigating how the three-dimensional patterns by which individual polyps grow combine to result in the creation of a whole coral head over time.

REFERENCES

Ashi J (1997) Computed Tomography scan image analysis of sediments. Proceedings of the Ocean Drilling Program, Scientific Results 156:151-159

Barnes DJ (1970) Coral Skeletons - An Explanation of their growth and structure. Science 170:1305-1308

Barnes DJ, Devereux MJ (1988) Variations in skeletal architecture associated with density banding in the hard coral *Porites*. J Exp Mar Biol Ecol 121:37-54

Barnes RD (1974) Invertebrate Zoology. W.B. Saunders Company, Philadelphia, PA, 117-136

Bessat F, Buigues D (2001) Two Centuries of variation in coral growth in a massive *Porites* colony from Moorea (French Polynesia): A response of ocean-atmosphere variability from South Central Pacific. Palaeogeogr Palaeocl 175:381-392

Boespflug X, Long BFN, Occhietti S (1995) Cat-scan in marine stratigraphy - A Quantitative Approach. Marine Geology 122:281-301

Bosscher H (1993) Computerized-tomography and skeletal density of coral skeletons. Coral Reefs 12:97-103

Brooks RA, Dichiro G (1976) Principles of computer-assisted tomography (Cat) in Radiographic and Radioisotopic Imaging. Phys Med Biol 21:689-732

Buddemeier, RW, Maragos JE, Knutson DW (1974) Radiographic studies of reef coral exoskeletons - rates and patterns of coral growth. J Exp Mar Biol Ecol 14:179-200

Burke L, and J. Maidens (2004) Reefs at risk in the Caribbean. World Resources Institute, Washington D.C

Cantin NE, Cohen AL, Karnauskas KB, Tarrant AM, McCorkle DC (2010) Ocean warming slows coral growth in the Central Red Sea. Science 329:322-325

Carpenter KE, Abrar M, Aeby G, Aronson RB, Banks S, Bruckner A, Chiriboga A, Cortes J, Delbeek JC, DeVantier L, Edgar GJ, Edwards AJ, Fenner D, Guzman HM, Hoeksema BW, Hodgson G, Johan O, Licuanan WY, Livingstone SR, Lovell ER, Moore JA, Obura DO, Ochavillo D, Polidoro BA, Precht WF, Quibilan MC, Reboton C, Richards ZT, Rogers AD, Sanciangco J, Sheppard A, Sheppard C, Smith J, Stuart S, Turak E, Veron JEN, Wallace C, Weil E, Wood E (2008) One-third of reef-building corals face elevated extinction risk from climate change and local impacts. Science 321:560-563

Carriquiry JD, Horta-Puga G (2010) The Ba/Ca record of corals from the Southern Gulf of Mexico: Contributions from land-use changes, fluvial discharge and oil-drilling muds. Mar Pollut Bull 60:1625-1630

Chen TR, Yu KF, Li S, Chen TG, Shi Q (2011) Anomalous Ba/Ca signals associated with low temperature stresses in *Porites* corals from Daya Bay, Northern South China Sea. J Environ Sci-China 23:1452-1459

Cnudde V, Masschaele B, Dierick M, Vlassenbroeck J, Van Hoorebeke L, Jacobs P (2006) Recent progress in X-ray CT as a geosciences tool. Applied Geochemistry 21:826-832

Cohen AL, McConnaughey TA (2003) Geochemical perspectives on coral

mineralization. Biomineralization 54:151-187

Dodge RE (1982) Effects of drilling mud on the reef-building coral *Montastrea-annularis*. Mar Biol 71:141-147

Dodge RE, Jickells TD, Knap AH, Boyd S, Bak RPM (1984) Reef-building coral skeletons as chemical pollution (Phosphorus) indicators. Mar Pollut Bull 15:178-187

Dodge RE, Lang JC (1983) Environmental correlates of hermatypic coral (*Montastrea-annularis*) growth on the East-Flower-Gardens-Bank, Northwest Gulf of Mexico. Limnol Oceanogr 28:228-240

Duchesne MJ, Moore F, Long BF, Labrie J (2009) A rapid method for converting medical Computed Tomography scanner topogram attenuation scale to Hounsfield Unit scale and to obtain relative density values. Eng Geol 103:100-105

Dunbar R, and J. Cole (1993) Coral records of ocean-atmosphere variability: Report from the workshop on coral paleoclimate reconstruction. NOAA Climate and Global Change Program Special Report 38

Gardner TA, Cote IM, Gill JA, Grant A, Watkinson AR (2003) Long-term region-wide declines in Caribbean corals. Science 301:958-960

Goreau TF (1959) The Physiology of skeleton formation in corals .1. A method for measuring the rate of calcium deposition by corals under different conditions. Biol Bull 116:59-75

Goreau TF, Goreau NI (1959) The physiology of skeleton formation in corals .2.

Calcium deposition by hermatypic corals under various conditions in the reef. Biol Bull 117:239-250

Houndfield GN (1973) Computerized transverse axial scanning (tomography) .1. Description of system. Brit J Radiol 46:1016-1022

Hudson JH, Shinn EA, Halley RB, Lidz B (1976) Sclerochronology - Tool for interpreting past environments. Geology 4:361-364

Hughes TP, Baird AH, Bellwood DR, Card M, Connolly SR, Folke C, Grosberg R, Hoegh-Guldberg O, Jackson JBC, Kleypas J, Lough JM, Marshall P, Nystrom M, Palumbi SR, Pandolfi JM, Rosen B, Roughgarden J (2003) Climate change, human impacts, and the resilience of coral reefs. Science 301:929-933

Knutson DW, Smith SV, Buddemeier, RW (1972) Coral chronometers - seasonal growth bands in reef corals. Science 177:270-&

Kwiatkowski L, Cox PM, Economou T, Halloran PR, Mumby PJ, Booth BBB, Carilli J, Guzman HM (2013) Caribbean coral growth influenced by anthropogenic aerosol emissions. Nat Geosci 6:362-366

Logan A, Anderson IH (1991) Skeletal extension growth-rate assessment in corals, using CT scan imagery. B Mar Sci 49:847-850

Lough JM (2008) 10th anniversary review: a changing climate for coral reefs. J Environ Monitor 10:21-29

Lough JM, Barnes DJ (1990) Intraannual timing of density band formation of *Porites* coral from the Central Great-Barrier-Reef. J Exp Mar Biol Ecol 135:35-57

Lough JM, Cooper TF (2011) New insights from coral growth band studies in an era

of rapid environmental change. Earth-Sci Rev 108:170-184

Milliman JD (1974) Recent Sedimentary Carbonates, Part 1: Marine Carbonates. Springer-Verlag, Berlin

Miner A (2013) Coral isotope record of environmental change in the Northwest Gulf of Mexico. M.S. thesis, Texas A&M University, College Station TX. p106

Nettleton L (1957) Gravity survey over a Gulf Coast continental shelf mound. Geophysics 12:630-642

Pandolfi JM, Bradbury RH, Sala E, Hughes TP, Bjorndal KA, Cooke RG, McArdle D, McClenachan L, Newman MJH, Paredes G, Warner RR, Jackson JBC (2003) Global trajectories of the long-term decline of coral reef ecosystems. Science 301:955-958

Rezak R, T. J. Bright, D. W. McGrail (1985) Reefs and Banks of the Northwestern Gulf of Mexico. John Wiley and Sons, Inc, New York. p259

Rosset A, Spadola L, Ratib O (2004) OsiriX: An open-source software for navigating in multidimensional DICOM images. Journal of Digital Imaging 17:205-216

Saadat K, Rahimpour-Bonab, H., Esfahani, M.R., and J. Vali (2011) Empirical correlation for porpsity deduction from X-ray computed tomography (CT). J Geope 1:47-54

Schmahl GP, Hickerson, E.L., and W. F. Precht (2008) Biology and ecology of coral reefs and coral communities in the Flower Garden Banks Region, Northwestern Gulf of Mexico. In: Coral Reefs of the USA. Springer Science + Business Media, Dania Beach Florida. B. Riegl and Dodge RE (eds) pp221-

226

Schneider CA, Rasband WS, Eliceiri KW (2012) NIH Image to ImageJ: 25 years of image analysis. Nature Methods 9:671-675

Smith TJ, Hudson JH, Robblee MB, Powell GVN, Isdale PJ (1989) Fresh-water flow from the Everglades to Florida Bay - A historical reconstruction based on fluorescent banding in the coral *Solenastrea-Bournoni*. B Mar Sci 44:274-282

Vernon J (2000a) Corals of the world, Vol 1. Australian Institute of Marine Science, Townsville, Australia: 47-56

Vernon J (2000b) Corals of the world, Vol 3. Australian Institute of Marine Science, Townsville, Australia: 212-225

Wagner AJ (2009) Oxygen and Carbon isotopes and coral growth in the Gulf of Mexico and Caribbean Sea and environmental and climate indicators. Ph.D. thesis. Texas A&M University, College Station TX, p117

Wellington SL, Vinegar HJ (1987) X-Ray Computerized-Tomography. J Petrol Technol 39:885-898

Wilkinson C (2008) Status of coral reefs of the world: 2008. Global Coral Reef Monitoring Network Reef and Rainforest Research Centre, Townsville, Australia. p304

Wilson JL (1975) Carbonate facies in geologic history. Springer-Verlag, Berlin

APPENDIX 1: DETAILED METHODS

Computed axial tomography methods

Each coral core was individually scanned using a CT Scan at the Texas A&M University Veterinary Science School, College Station, TX. The medical CT scanner used was a Siemens SOMATOM Definition AS, 40-slice CT with a resolution of 0.6 mm. Each core was placed at a random x-y orientation on the CT bed, but with the top of the core pointed towards the CT source. All orientations of slices digitally created are relative to the initial position of the specific core. The WFGB NW, SW, and SE-A cores were digitally sliced at four different orientations relative to the initial position of the core: 0°, 45°, 90°, and 135°. The rest of the WFGB and EFGB cores were digitally sliced at 0°, 45°, and 90° orientations, relative to the longitudinal z-axis. All of the core sections also had a transverse orientation, moving along the z-axis of the core at 0.6 mm intervals.

Once all of the raw CT data was acquired, DVD's of the data were taken back to the Oceanography Department at Texas A&M University and imported into the OSIRIX DICOM viewer, medical software (http://www.osirix-viewer.com/) to analyze. All actual polyp extension rates were calculated using OsiriX as well as all 3D representations. The files from OsiriX were exported into .tif files and imported into the free software ImageJ (http://rsb.info.nih.gov/ij/) to calculate the conventional extension rates.

Measuring conventional extension rates

Measuring the conventional extension rates was completed using .tif files of 0.6 mm resolution from OsiriX software, uploaded into the ImageJ 64bit Program. This was completed for each core section at each orientation. Three straight ROI (region of interest) transect lines were drawn across the 23rd 0.6 mm slice of each orientation to measure the pixel gradient on a single slice, each transect line was drawn to follow the polyp growth axis as closely as possible as well as remain as perpendicular as possible to the growth bands. For each individual transect a gray scale plot was created showing the pixel value vs. the distance across the core in the z-direction. By exporting the data from the produced gray scale plot; the data was graphed in Excel. Based upon the peaks in the excel-produced gray scale plot, the distance between high-density bands could be determined, i.e. the annual extension rate of the coral. The exact point of the highest density within a high-density band was determined.

Additionally, a "traditional" digital X-ray was created digitally by finding the average intensity of slices 20-34 (14 slices at 0.6 mm to get an approximate conventional X-ray 8.4 mm thick) of each core at each given orientation and taking the same three ROI transects as on the single slice. Therefore each single orientation of a core would end up with 6 transect lines (3 across a single 0.6 mm slice and 3 across the created X-ray). This enables a comparison between a single slice gray scale plot and a generated X-ray gray scale plot as well as how the extension rate changed across the different transects. The gray scale plots generated by ImageJ reflect the relative density of the core at any given location. The higher the pixel value the higher the density, so by

determining the location of the highest densities across a core, the annual growth bands are determined.

Actual coral polyp extension rates

Once the raw DICOM data is uploaded in OsiriX, the transverse slices across the z-axis of the core are used to follow the individual polyp extension. The growth bands show up as bright waves moving across the core and by adjusting the gray scale these become more obvious. The x-y coordinates and slice number of the individual polyp were recorded as it passed through each subsequent growth band, ignoring the first partial year (2012).

The actual extension rate was calculated using the x- and y-coordinates of each polyp at a high-density band and creating the z-coordinate by knowing the slice number and the distance between slices (0.6 mm). This allows for computing the 3D movement of the coral and discovering the actual distance the individual polyp grew. This was completed on each core section for three individual polyps. The actual polyp movement was calculated based on Pythagorean theorem in a 3D area, using $x^2+y^2=c^2$ to find the 2D movement between the changing x and y coordinates of a polyp. From there, used $s^2= c^2+z^2$ to calculate the movement of the polyp in 3D space.

Analysis

Once all the data had been acquired for each core (actual and conventional extension rates), it was input into an excel database. From this point, all analyses were

computed. Each CT scan remained archived within the OsiriX software. Each transect for each core was compiled for the varying orientations of the slabs and slices. For each slice and each slab, averages were taken of each of the three transects to determine the average extension rates for each year across any given orientation. Averages of individual polyp rates within a single core were also taken. This helps to establish how much actual coral polyp extension rates differ from one another as well as how extension rates vary between cores.

APPEDIX II: CORE DESCRIPTIONS

NOAA Flower Gardens Banks National Marine Sanctuary collected ten coral cores under the permit number FGBNMS-2009-001.

Core collection locations

At the WFGB the center buoy is located at 27°52'30.6" N, 93°48'54.1" W, and each core was taken at specific degree intervals from the markers at each of the four corners of the 100 m x 100 m study site. The following are the positions of each core location: WFGB SW core was taken 10.3 m from the south west corner marker at a 50° bearing at a depth of 71 ft; WFGB SE core was taken 14.2 m from the center marker at a 100° bearing at a depth of 66 ft; WFGB NW core was taken 5.6 m from the NE25 marker at a 180° bearing at a depth of 65 ft; WFGB NE core was taken 7.9 m from the North C marker at a 85° bearing at a depth of 65 ft. The WFGB SW core has two sections; WFGB SW-B was not analyzed due to an equipment malfunction during the drilling process. The WFGB SE core also has two sections, SE-A was cut short due to a fossilized disruption, SE-B was taken from the same location to have a longer core without the fossilized disruption, and both are analyzed.

The center buoy at the EFGB is located at 27°54'31.9" N, 93°35'49.0" W. This study area is also 100 m x 100 m large and each core was taken at a bearing from each corner. The following are the positions of each core location: The EFGB NE core was taken 7.8 m from the N25 marker at 120° bearing at depth of 60 ft; the EFGB NW core was taken 12.1 m from the North C marker at 285° bearing at depth of 72 ft; the EFGB

SE core was taken 15.9 m from the SE corner marker at 300° bearing at depth of 60 ft; the EFGB SW core was taken 7.5 m from the South C marker at 355° bearing at depth of 62 ft. The EFGB SW core broke in half during the coring process, the top section of the core will be called EFGB SW-Top and the bottom section will be called EFGB SW-Bottom. EFGB NW was not analyzed due to the polyp growth being too difficult to follow for actual extension rates; the core was taken as the polyps were budding.

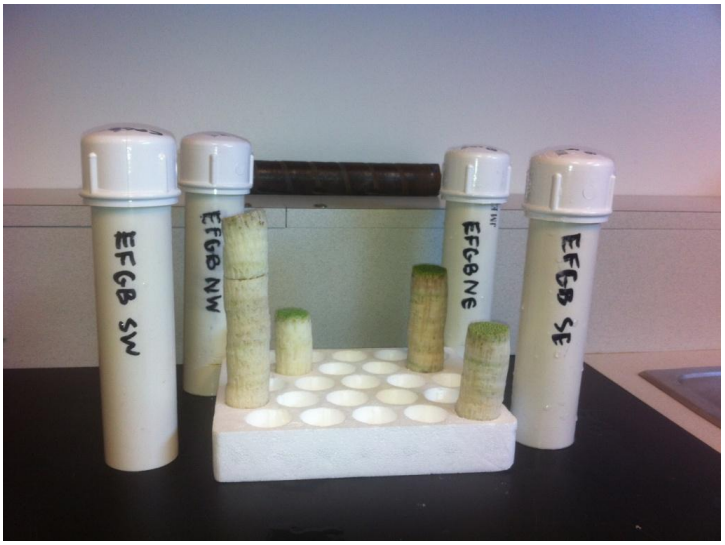

Figure A1: The East Flower Garden Bank Coral Cores, photo courtesy of NOAA National Marine Sanctuary Personnel

Figure A2: The West Flower Garden Bank Coral Cores, photo courtesy of NOAA National Marine Sanctuary Personnel

APPENDIX III: CT SCAN IMAGES AND TRANSECT LOCATIONS

The following results are presented through an assemblage of figures (Figures A3-A20). Each core has two sets of figures and three tables. The first figure for each core shows the approximate locations of the three transects used for measuring the annual extension rates for the individual 0.6 mm slices at varying orientations 0°, 45°, 90° and, in some, 135°. The second figure presented for each core shows the digitally created slab at each orientation and the approximate locations of the three transects used for the annual extension measurements. Each slab is the average pixel intensity of 14 single 0.6 mm slices, produced to represent the traditional X-ray image.

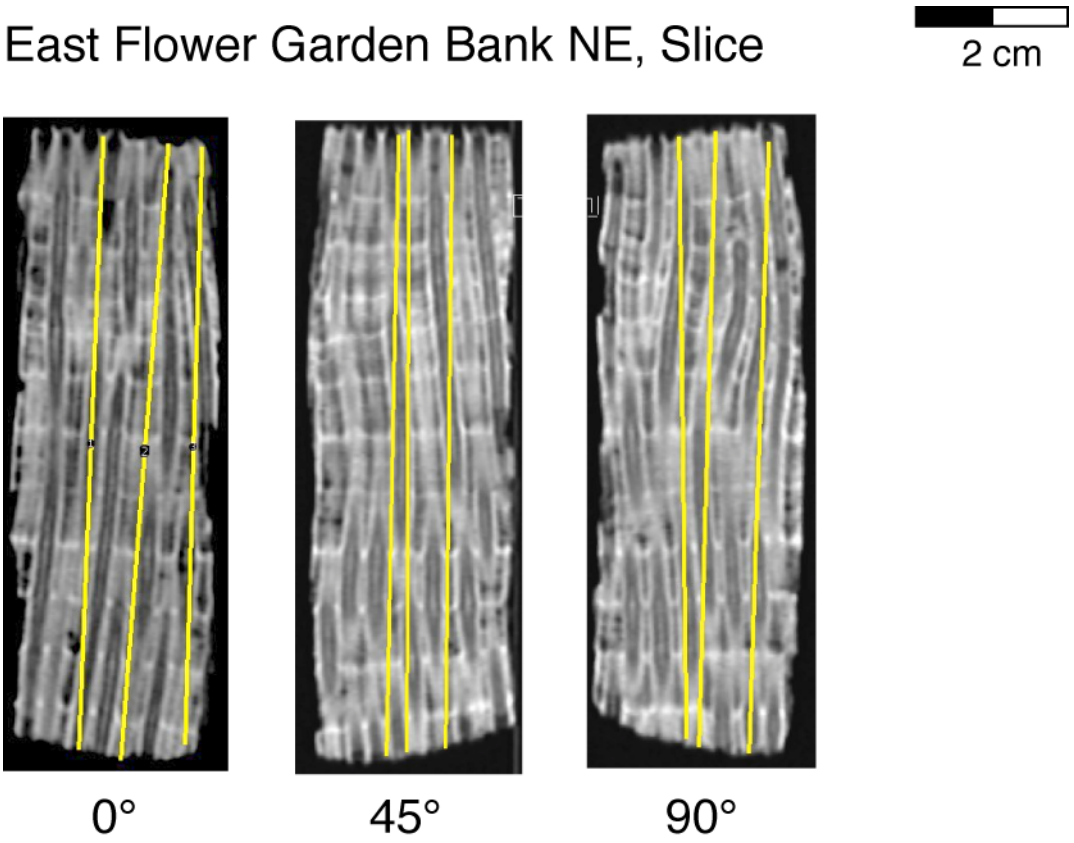

Figure A3: Images of the approximate locations of the three transects (yellow lines) across the 0.6 mm individual slices at orientations 0°, 45° and 90° of the EFGB NE core.

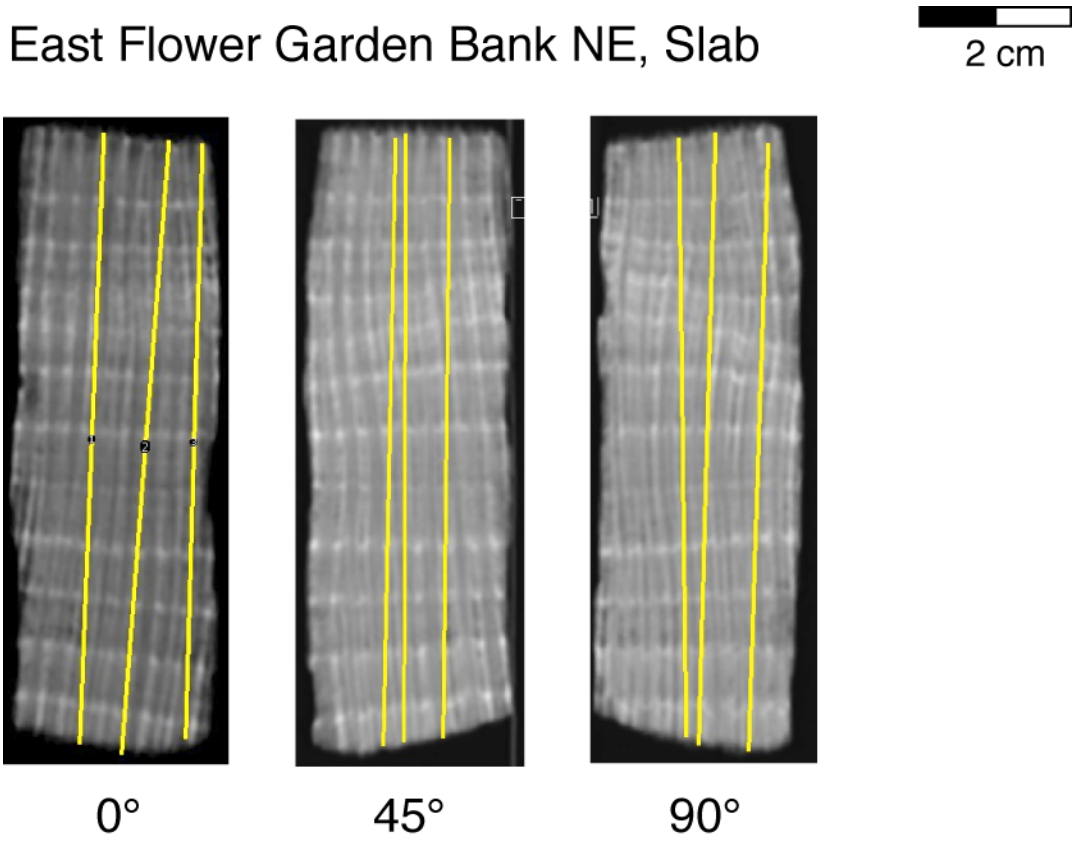

Figure A4: Images of the approximate locations of the three transects (yellow lines) across the digitally created slab at orientations 0°, 45° and 90° of the EFGB NE core.

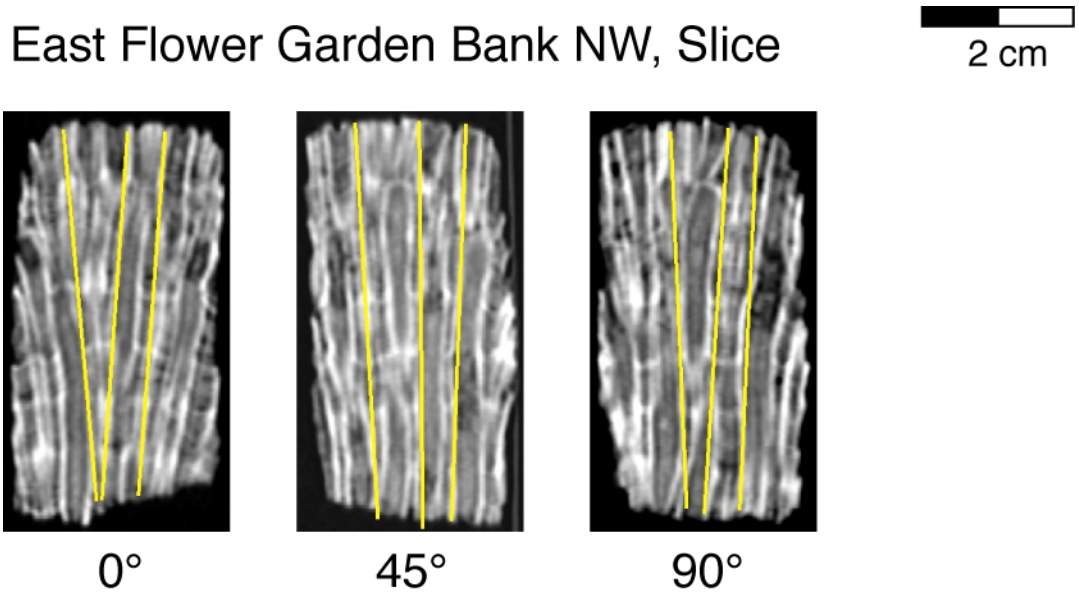

Figure A5: Images of the approximate locations of the three transects (yellow lines) across the 0.6 mm individual slices at orientations 0°, 45° and 90° of the EFGB NW core.

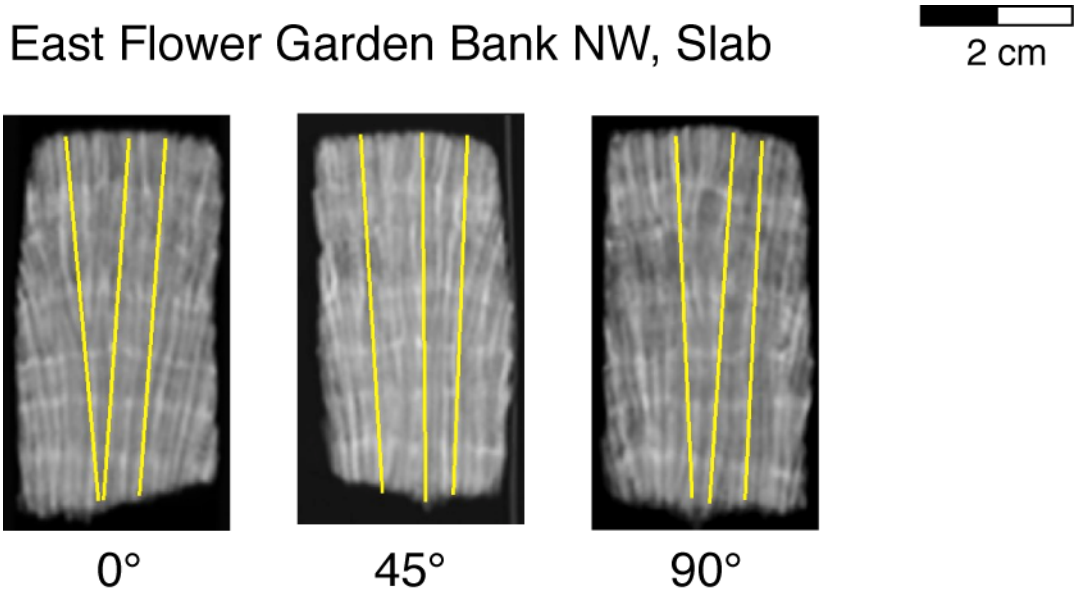

Figure A6: Images of the approximate locations of the three transects (yellow lines) across the digitally created slab at orientations 0°, 45° and 90° of the EFGB NW core.

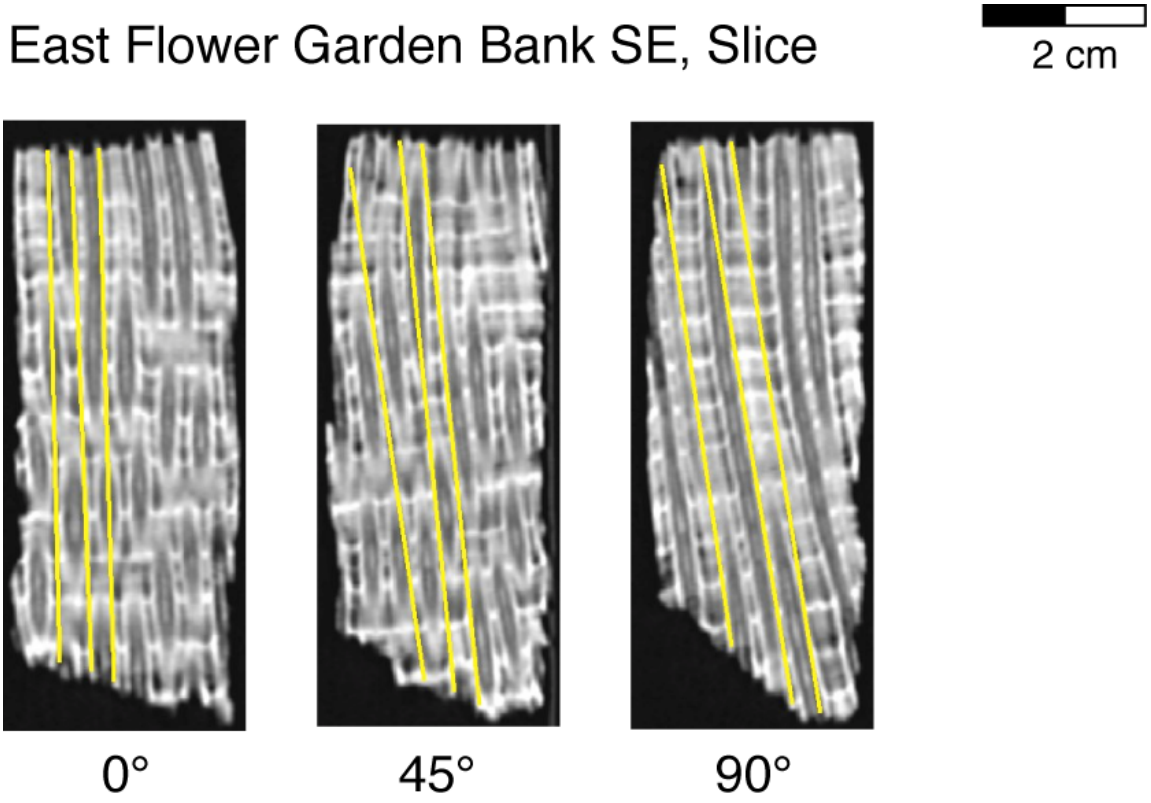

Figure A7: Images of the approximate locations of the three transects (yellow lines) across the 0.6 mm individual slices at orientations 0°, 45° and 90° of the EFGB SE core.

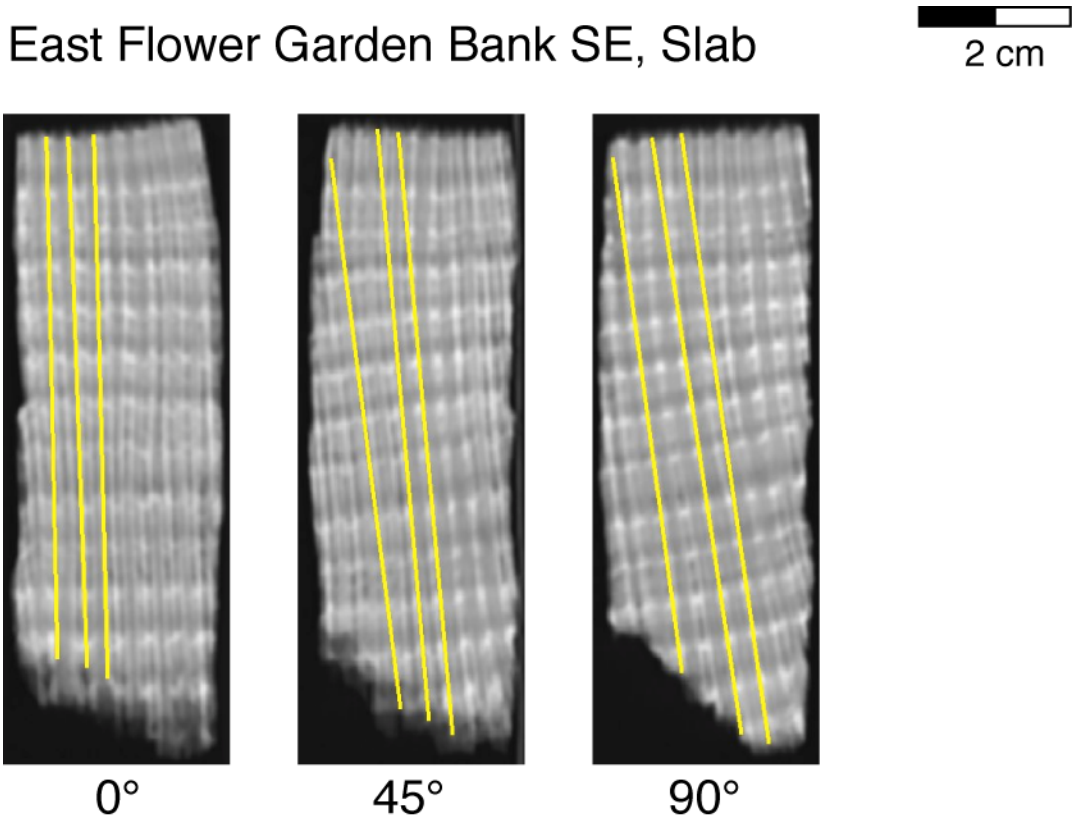

Figure A8: Images of the approximate locations of the three transects (yellow lines) across the digitally created slab at orientations 0°, 45° and 90° of the EFGB SE core.

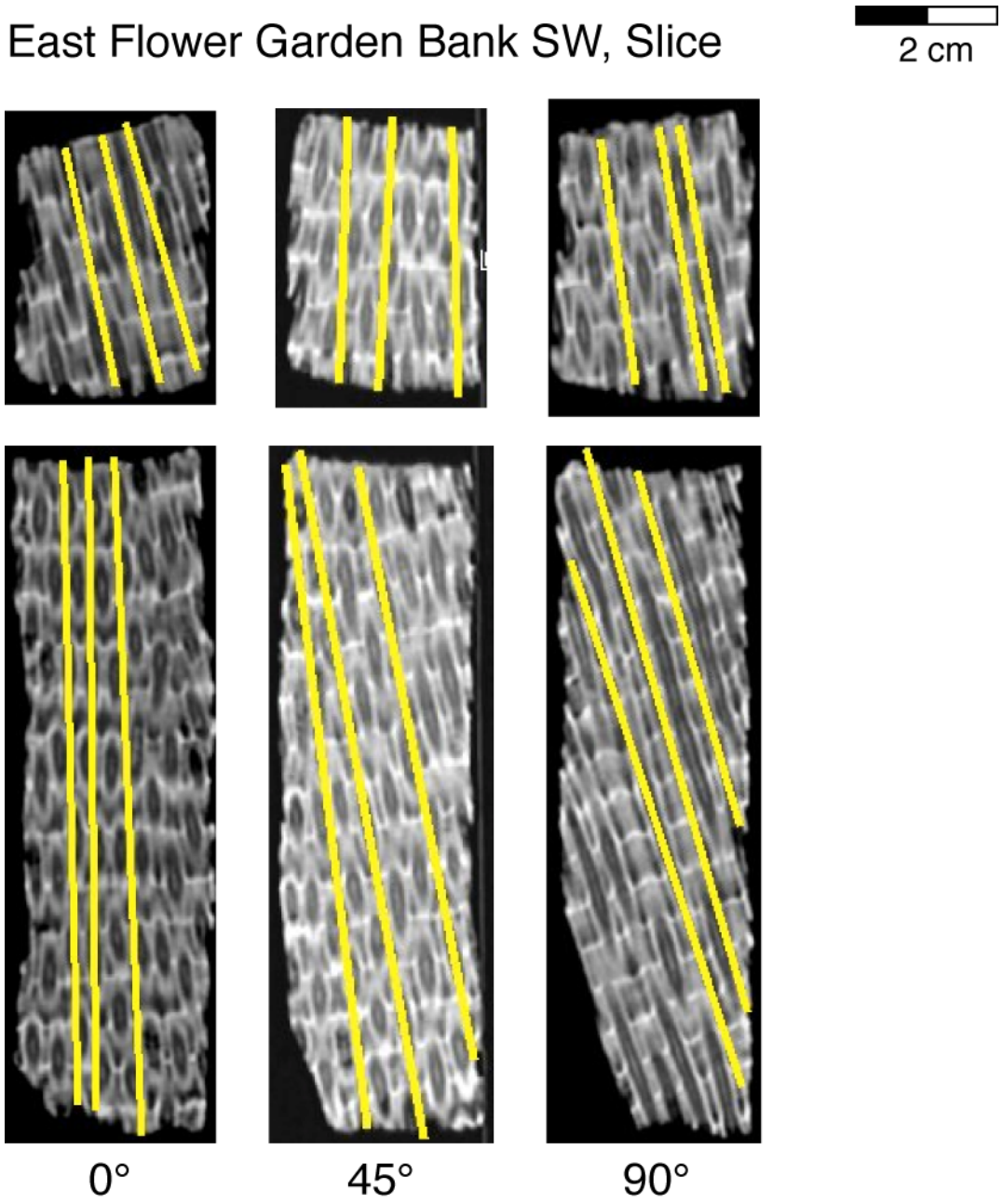

Figure A9: Images of the approximate locations of the three transects (yellow lines) across the 0.6 mm individual slices at orientations 0°, 45° and 90° of the EFGB SW core, both the top and bottom sections of the core.

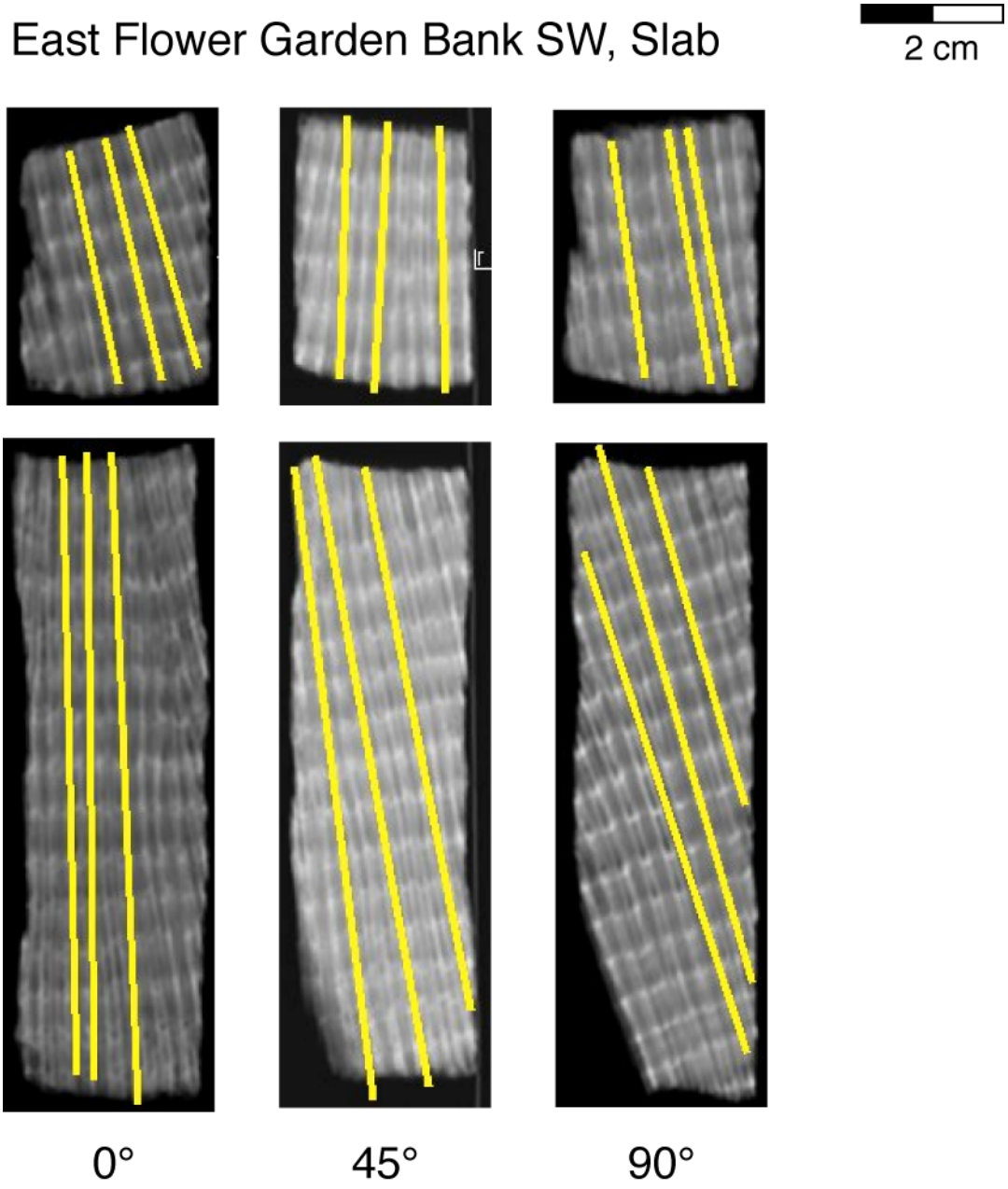

Figure A10: Images of the approximate locations of the three transects (yellow lines) across the digitally created slab at orientations 0°, 45° and 90° of the EFGB SW core, both top and bottom sections.

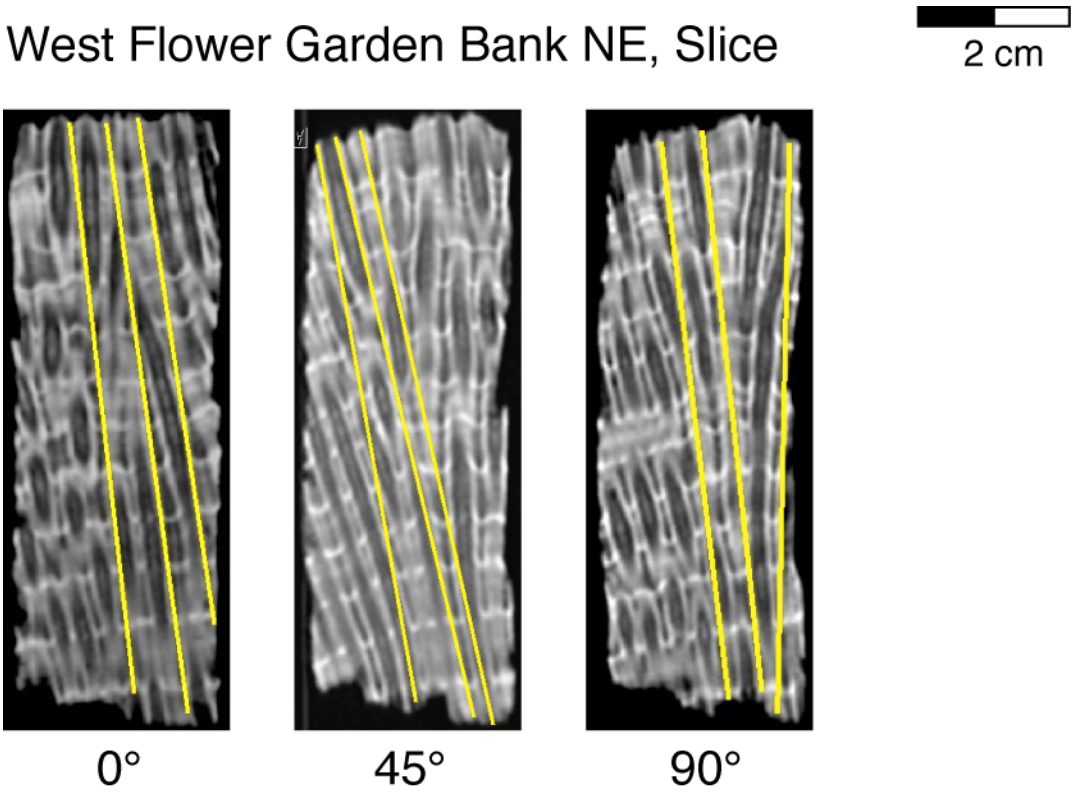

Figure A11: Images of the approximate locations of the three transects (yellow lines) across the 0.6 mm individual slices at orientations 0°, 45° and 90° of the WFGB NE core.

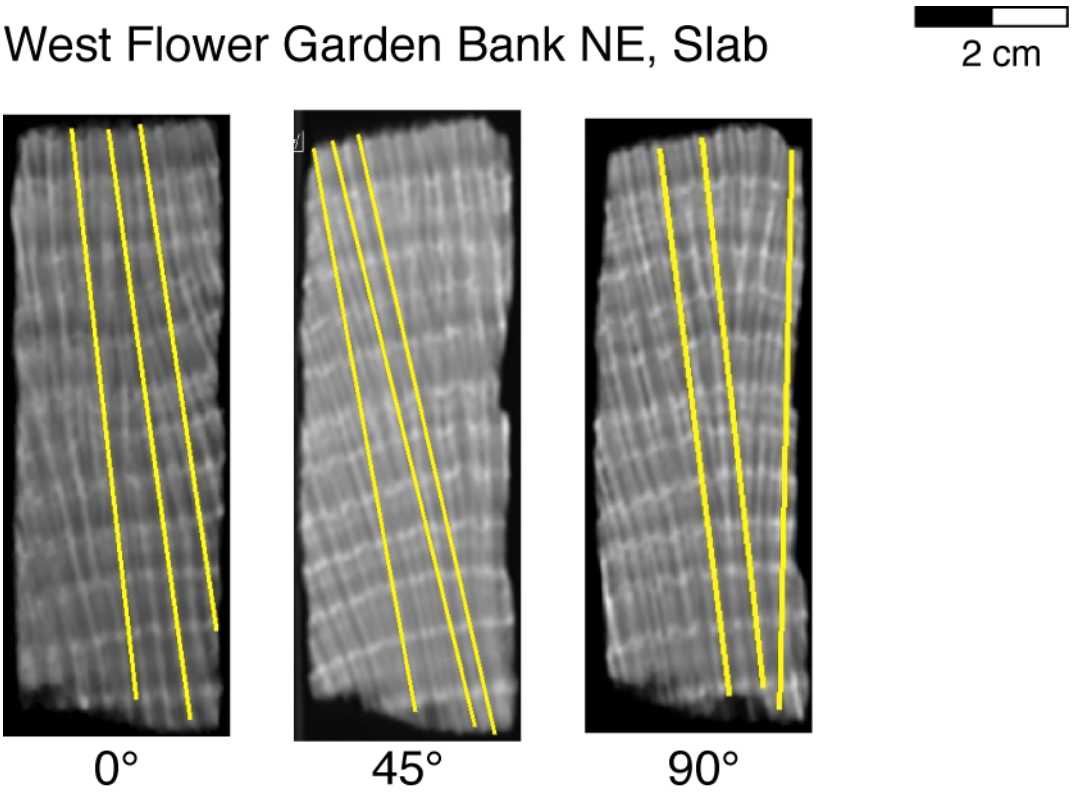

Figure A12: Images of the approximate locations of the three transects (yellow lines) across the digitally created slab at orientations 0°, 45° and 90° of the WFGB NE core.

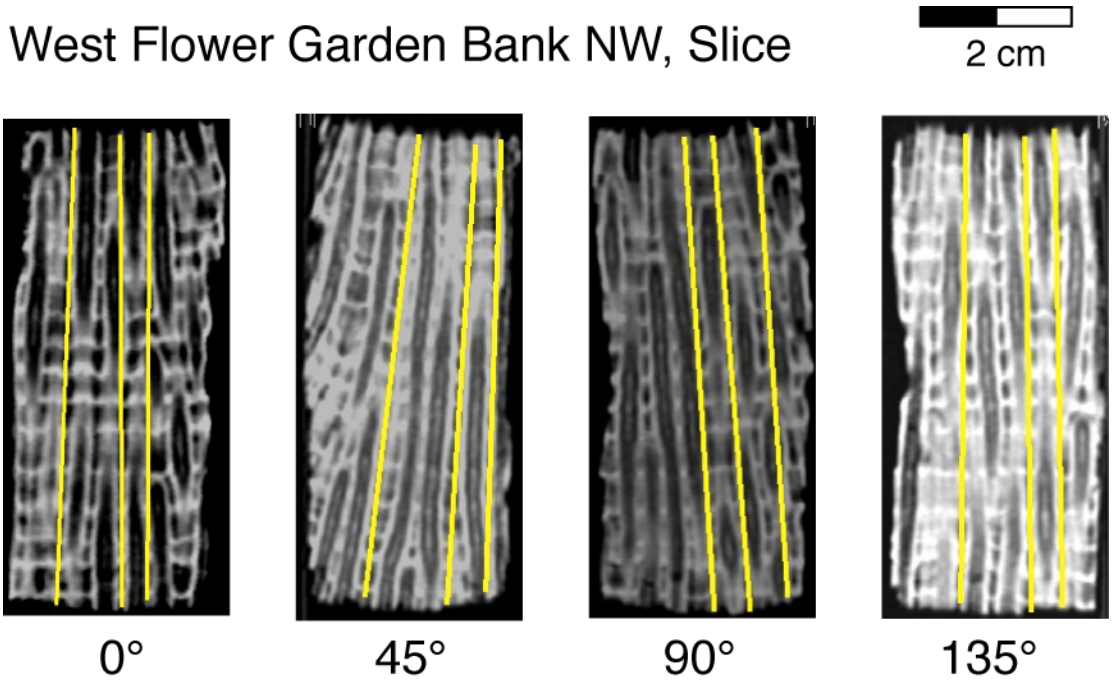

Figure A13: Images of the approximate locations of the three transects (yellow lines) across the 0.6 mm individual slices at orientations 0°, 45°, 90° and 135° of the WFGB NW core.

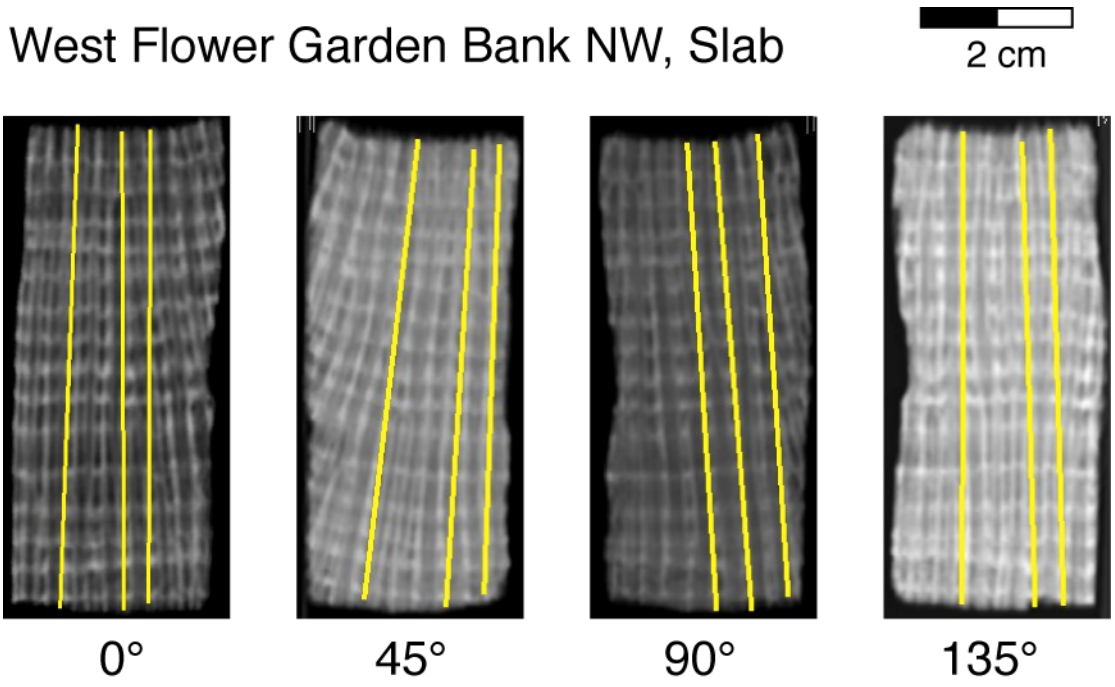

Figure A14: Images of the approximate locations of the three transects (yellow lines) across the digitally created slab at orientations 0°, 45°, 90° and 135° of the WFGB NW core.

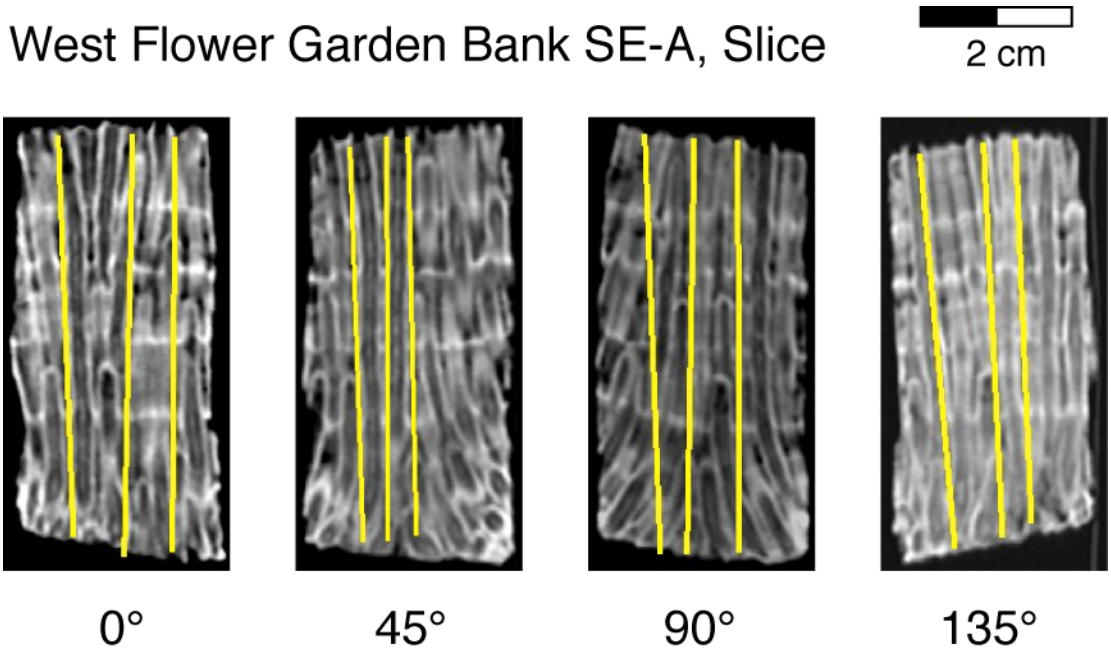

Figure A15: Images of the approximate locations of the three transects (yellow lines) across the 0.6 mm individual slices at orientations 0°, 45°, 90° and 135° of the WFGB SE-A core.

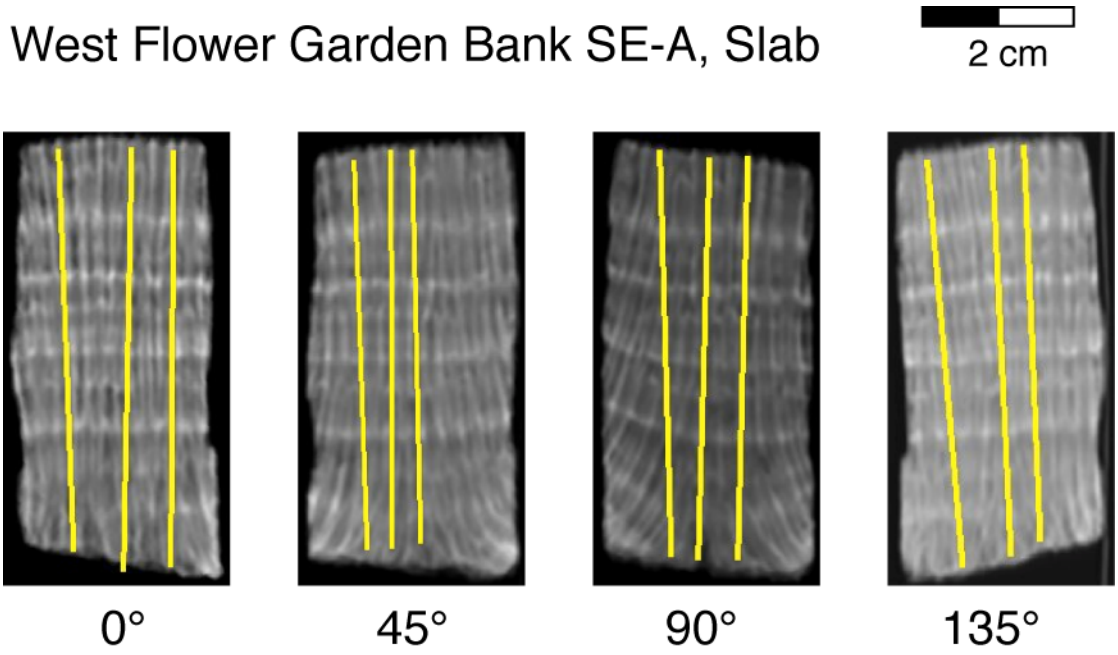

Figure A16: Images of the approximate locations of the three transects (yellow lines) across the digitally created slab at orientations 0°, 45°, 90° and 135° of the WFGB SE-A core.

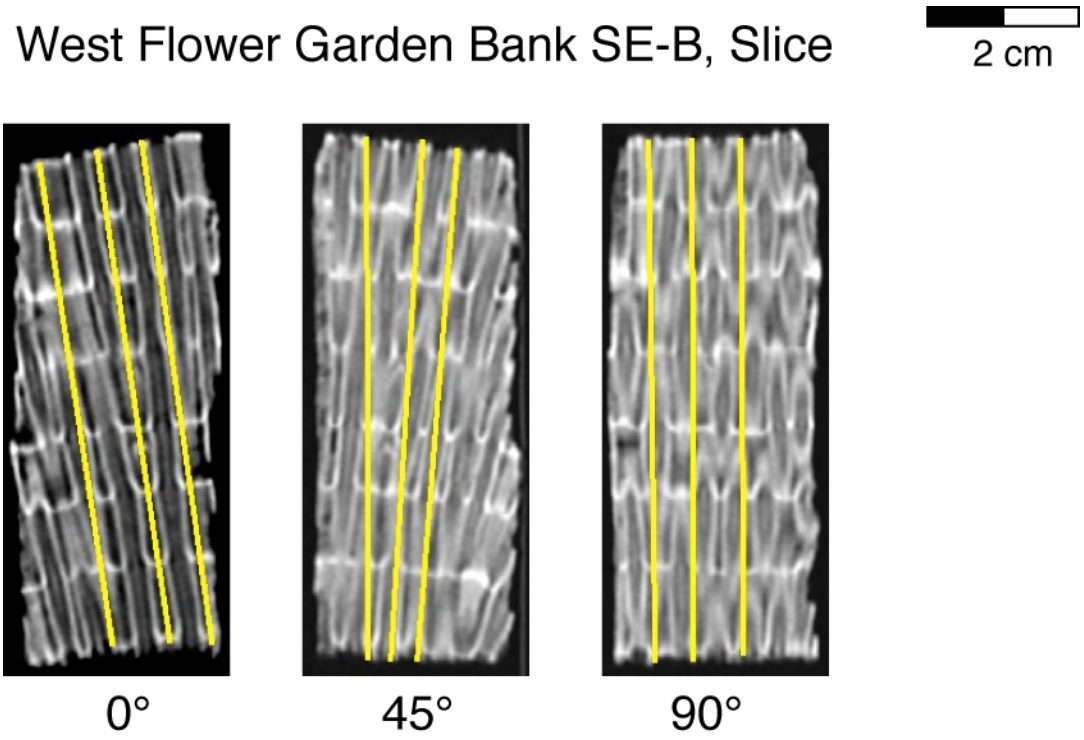

Figure A17: Images of the approximate locations of the three transects (yellow lines) across the 0.6 mm individual slices at orientations 0°, 45° and 90° of the WFGB SE-B core

Figure A18: Images of the approximate locations of the three transects (yellow lines) across the digitally created slab at orientations 0°, 45° and 90° of the WFGB SE-B core.

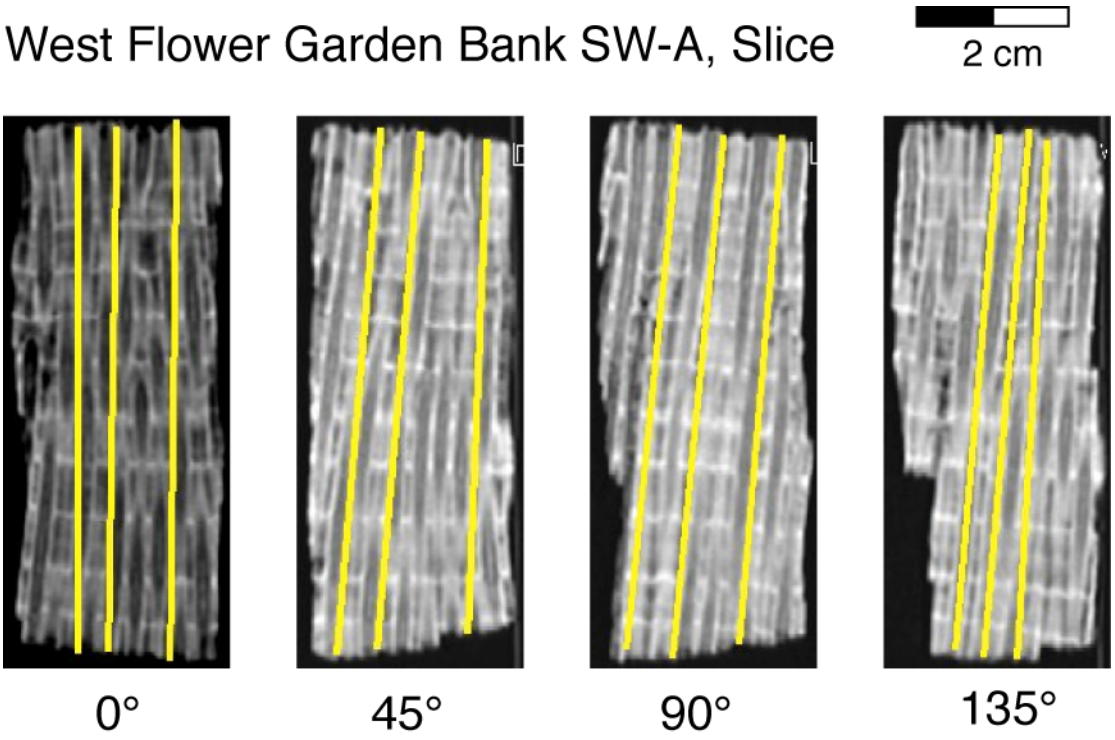

Figure A19: Images of the approximate locations of the three transects (yellow lines) across the 0.6 mm individual slices at orientations 0°, 45°, 90° and 135° of the WFGB SW-A core.

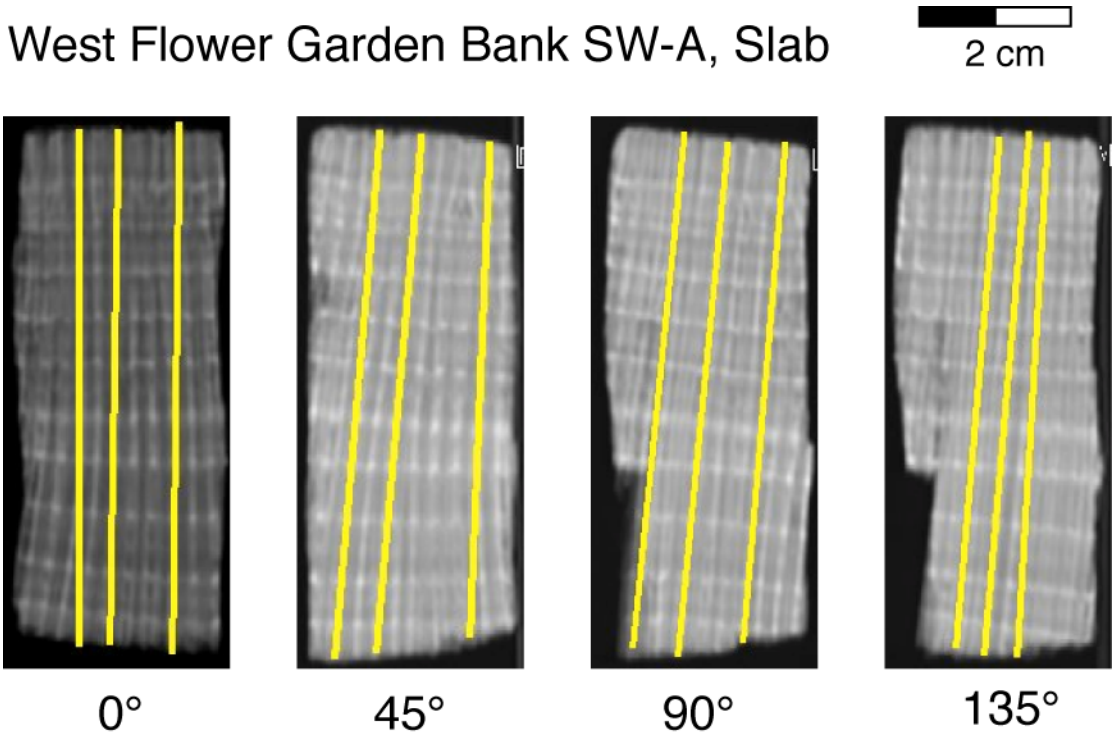

Figure A20: Images of the approximate locations of the three transects (yellow lines) across the digitally created slab at orientations 0°, 45°, 90° and 135° of the WFGB SW-A core.

APPENDIX IV: ANNUAL AVERAGE EXTENSION RATES

Associated with each set of figures in Appendix III are two tables. For each core there is a table showing the average measured extension for each set of slice images and a table for each set of slab images. Any blank spots in the table are associated with no measured extension rate for that year at the specific orientation. Additionally, the last two tables, Tables A19 and A20, show the average measured actual polyp extension rates across all the cores. All results are presented in centimeters and the estimated time intervals begin in July of 2012 (the date of collection).

Table A1: East Flower Garden Bank northeast core average annual extension across the single 0.6mm slice orientations of 0°, 45° and 90° in mm/year.

Year	Estimated Time Interval	0°	45°	90°
1	2012-2011	3.70	6.37	5.82
2	2011-2010	9.32	6.02	5.57
3	2010-2009	7.02	7.08	6.98
4	2009-2008	5.87	4.70	5.36
5	2008-2007	5.87	8.35	4.91
6	2007-2006	7.52	8.65	9.26
7	2006-2005	7.80	9.41	8.90
8	2005-2004	9.36	6.68	9.56
9	2004-2003	6.74	6.58	6.73
10	2003-2002	8.17	7.84	6.63
11	2002-2001	9.86	8.04	6.88
12	2001-2000			8.58

Table A2: East Flower Garden Bank northeast core average annual extension across the slab orientations of 0°, 45° and 90° in mm/year.

Year	Estimated Time Interval	0°	45°	90°
1	2012-2011	6.00	7.79	2.33
2	2011-2010	7.10	6.43	4.55
3	2010-2009	7.06	6.83	7.59
4	2009-2008	5.75	4.91	6.83
5	2008-2007	5.83	6.42	5.11
6	2007-2006	7.47	8.60	6.42
7	2006-2005	8.42	8.65	8.60
8	2005-2004	8.30	8.25	9.56
9	2004-2003	7.72	7.23	7.44
10	2003-2002	7.64	7.79	7.49
11	2002-2001	8.05	7.69	8.25
12	2001-2000			7.84

Table A3: East Flower Garden Bank northwest core average annual extension across the single 0.6mm slice orientations of 0°, 45° and 90° in mm/year.

Year	Estimated Time Interval	0°	45°	90°
1	2012-2011	6.65	6.86	7.84
2	2011-2010	7.05	7.19	6.80
3	2010-2009	8.10	8.64	8.54
4	2009-2008	9.45	7.64	6.64
5	2008-2007	6.78	8.80	7.92
6	2007-2006	7.83	11.47	9.69

Table A4: East Flower Garden Bank northwest core average annual extension across the slab orientations of 0°, 45° and 90° in mm/year.

Year	Estimated Time Interval	0°	45°	90°
1	2012-2011	9.06	7.60	7.63
2	2011-2010	5.82	7.36	6.97
3	2010-2009	6.26	6.78	7.63
4	2009-2008	9.67	9.26	10.35
5	2008-2007	7.40	6.78	6.31
6	2007-2006	7.83	9.46	6.85

Table A5: East Flower Garden Bank southeast core average annual extension across the single 0.6mm slice orientations of 0°, 45° and 90° in mm/year.

Year	Estimated Time Interval	0°	45°	90°
1	2012-2011	2.57	2.55	2.24
2	2011-2010	4.04	4.58	6.09
3	2010-2009	4.75	5.37	6.15
4	2009-2008	5.03	4.95	5.83
5	2008-2007	5.85	5.94	5.42
6	2007-2006	5.36	5.05	6.15
7	2006-2005	6.50	4.90	5.99
8	2005-2004	5.08	5.63	5.63
9	2004-2003	10.00	6.61	5.94
10	2003-2002	5.85	5.68	5.63
11	2002-2001	6.01	5.62	5.52
12	2001-2000	6.72	5.89	5.36
13	2000-1999		5.94	5.47
14	1999-1998		3.28	5.16

Table A6: East Flower Garden Bank southeast core average annual extension across the slab orientations of 0°, 45° and 90° in mm/year.

Year	Estimated Time Interval	0°	45°	90°
1	2012-2011	2.35	2.03	3.02
2	2011-2010	4.48	4.95	5.42
3	2010-2009	5.19	5.42	5.52
4	2009-2008	4.43	5.21	5.89
5	2008-2007	5.74	5.89	5.83
6	2007-2006	5.79	6.20	6.09
7	2006-2005	6.28	5.73	6.15
8	2005-2004	5.74	5.78	6.15
9	2004-2003	7.16	6.51	5.52
10	2003-2002	5.30	5.62	5.42
11	2002-2001	6.34	5.63	5.42
12	2001-2000	6.23	5.37	5.26
13	2000-1999		5.16	5.42
14	1999-1998			4.69

Table A7: East Flower Garden Bank southwest core average annual extension across the single 0.6mm slice orientations of 0°, 45° and 90° in mm/year.

Year	Estimated Time Interval	0°	45°	90°
1	2012-2011	8.89	8.16	7.35
2	2011-2010	5.97	5.14	6.70
3	2010-2009	6.83	9.46	6.60
4	2009-2008	6.94	7.15	7.14
5	2008-2007	7.38	7.45	7.24
6*	2007-2006	4.99	4.43	2.70
7*	2006-2005	6.51	5.84	7.14
8	2005-2004	7.38	6.44	6.70
9	2004-2003	6.62	7.15	5.95
10	2003-2002	7.38	4.43	7.68
11	2002-2001	5.53	9.46	9.30
12	2001-2000	5.86	7.35	7.03
13	2000-1999	5.97	8.46	6.70
14	1999-1998	6.29	6.65	6.81
15	1998-1997	8.46	8.66	7.03
16	1997-1996	6.83	3.83	7.14
17	1996-1995	7.05	7.95	6.00
18	1995-1994	7.05	4.93	6.81
19	1994-1993	6.07	5.74	5.84
20	1993-1992			6.16

*Note: Years 6 and 7 are skewed due to the breakage between the top and bottom sections of the core. The annual extension rates for years 6 and 7 were measured as accurately as possible

Table A8: East Flower Garden Bank southwest core average annual extension across the slab orientations of 0°, 45° and 90° in mm/year.

Year	Estimated Time Interval	0°	45°	90°
1	2012-2011	8.13	8.66	8.11
2	2011-2010	6.51	6.65	6.27
3	2010-2009	7.16	6.14	6.81
4	2009-2008	6.51	7.05	7.14
5	2008-2007	7.38	7.35	7.03
6*	2007-2006	5.21	3.63	4.76
7*	2006-2005	5.64	6.24	7.35
8	2005-2004	7.16	6.55	6.38
9	2004-2003	6.83	6.75	6.92
10	2003-2002	7.27	6.44	6.81
11	2002-2001	6.40	8.16	6.92
12	2001-2000	8.89	7.25	7.24
13	2000-1999	6.94	6.75	6.81
14	1999-1998	7.37	7.55	7.03
15	1998-1997	7.81	6.85	7.03
16	1997-1996	7.05	6.44	6.16
17	1996-1995	6.29	8.06	6.81
18	1995-1994	7.27	6.65	6.16
19	1994-1993	5.86	6.49	6.16
20	1993-1992			6.16

*Note: Years 6 and 7 are skewed due to the breakage between the top and bottom sections of the core. The annual extension rates for years 6 and 7 were measured as accurately as possible

Table A9: West Flower Garden Bank northeast core average annual extension across the single 0.6mm slice orientations of 0°, 45° and 90° in mm/year.

Year	Estimated Time Interval	0°	45°	90°
1	2012-2011	4.95	4.50	2.40
2	2011-2010	7.64	6.75	2.94
3	2010-2009	6.11	5.30	3.90
4	2009-2008	6.55	6.91	5.47
5	2008-2007	10.92	6.16	6.84
6	2007-2006	10.55	8.41	5.73
7	2006-2005	5.53	6.38	5.37
8	2005-2004	6.84	7.34	6.08
9	2004-2003	8.08	6.80	5.50
10	2003-2002	7.71	8.20	7.58
11	2002-2001	10.04	9.32	9.02

Table A10: West Flower Garden Bank northeast core average annual extension across the slab orientations of 0°, 45° and 90° in mm/year.

Year	Estimated Time Interval	0°	45°	90°
1	2012-2011	0.36	3.80	2.81
2	2011-2010	6.70	8.84	6.52
3	2010-2009	8.59	6.11	5.73
4	2009-2008	6.11	6.64	5.63
5	2008-2007	7.21	7.23	6.05
6	2007-2006	7.13	5.79	6.11
7	2006-2005	6.33	6.48	6.88
8	2005-2004	6.11	6.75	6.01
9	2004-2003	7.13	6.96	6.52
10	2003-2002	6.55	7.71	7.58
11	2002-2001	7.79	9.48	7.68
12	2001-2000	11.57		7.87

13 2000-1999 9.50

Table A11: West Flower Garden Bank northwest core average annual extension across the single 0.6mm slice orientations of 0°, 45°, 90° and 135° in mm/year.

Year	Estimated Time Interval	0°	45°	90°	135°
1	2012-2011	2.09	0.95	2.71	1.77
2	2011-2010	2.68	3.89	3.20	2.40
3	2010-2009	3.86	3.62	4.11	4.26
4	2009-2008	4.67	4.75	4.60	4.57
5	2008-2007	4.72	4.97	2.98	3.67
6	2007-2006	4.58	5.38	4.69	4.17
7	2006-2005	4.81	4.16	4.65	4.76
8	2005-2004	4.26	3.80	4.11	3.71
9	2004-2003	3.99	4.48	4.33	4.67
10	2003-2002	4.58	4.11	3.97	3.85
11	2002-2001	3.81	5.02	4.92	3.80
12	2001-2000	5.94	4.20	5.69	6.57
13	2000-1999	4.99	4.30	4.92	5.66
14	1999-1998	3.58	4.66	4.56	4.67
15	1998-1997	3.58	3.39	3.38	3.99
16	1997-1996	3.27		3.99	3.31
17	1996-1995	3.67			

Table A12: West Flower Garden Bank northwest core average annual extension across the slab orientations of 0°, 45°, 90° and 135° in mm/year.

Year	Estimated Time Interval	0°	45°	90°	135°
1	2012-2011	2.13	1.90	1.31	1.18
2	2011-2010	2.31	4.43	3.34	3.08
3	2010-2009	4.04	3.66	3.88	4.08
4	2009-2008	4.58	4.02	4.65	4.66
5	2008-2007	3.63	5.38	3.52	3.71
6	2007-2006	3.67	5.56	3.75	3.31
7	2006-2005	5.17	3.93	4.96	4.98
8	2005-2004	4.36	4.29	4.02	4.17
9	2004-2003	4.22	4.48	4.11	4.94
10	2003-2002	4.08	4.02	4.42	3.76
11	2002-2001	3.99	5.15	4.20	4.08
12	2001-2000	6.26	4.07	5.87	6.39
13	2000-1999	5.53	3.93	5.37	5.34
14	1999-1998	4.58	4.25	4.24	4.44
15	1998-1997	3.18	3.89	3.29	3.03
16	1997-1996	4.49	2.98	4.33	4.57

Table A13: West Flower Garden Bank southwest-A core average annual extension across the single 0.6mm slice orientations of 0°, 45°, 90° and 135° in mm/year.

Year	Estimated Time Interval	0°	45°	90°	135°
1	2012-2011	6.18	5.74	6.45	3.81
2	2011-2010	5.67	3.91	5.43	5.29
3	2010-2009	5.77	10.95	6.06	4.02
4	2009-2008	7.10	5.85	6.21	3.81
5	2008-2007	6.23	5.14	6.06	7.59
6	2007-2006	6.18	5.35	7.73	5.93
7	2006-2005	5.93	5.42	5.57	8.86
8	2005-2004	7.10	7.15	7.20	5.89
9	2004-2003	7.51	8.73	8.05	4.38
10	2003-2002	6.64	4.86	5.64	3.70
11	2002-2001				5.05
12	2001-2000				5.82

Table A14: West Flower Garden Bank southwest-A core average annual extension across the slab orientations of 0°, 45°, 90° and 135° in mm/year.

Year	Estimated Time Interval	0°	45°	90°	135°
1	2012-2011	6.33	6.44	6.45	3.00
2	2011-2010	5.57	5.04	5.39	5.68
3	2010-2009	5.93	6.16	6.17	6.32
4	2009-2008	5.88	5.99	6.21	6.07
5	2008-2007	6.49	7.01	6.14	6.49
6	2007-2006	7.25	6.30	7.45	4.02
7	2006-2005	5.72	6.02	5.67	5.12
8	2005-2004	7.10	6.20	7.23	6.03
9	2004-2003	7.77	10.21	7.91	6.14
10	2003-2002	5.77	4.79	5.75	6.17
11	2002-2001				5.57
12	2001-2000				4.45

Table A15: West Flower Garden Bank southeast-A core average annual extension across the single 0.6mm slice orientations of 0°, 45°, 90° and 135° in mm/year.

Year	Estimated Time Interval	0°	45°	90°	135°
1	2012-2011	6.90	10.96	7.45	9.19
2	2011-2010	9.84	12.03	9.57	8.08
3	2010-2009	9.57	7.29	13.04	9.51
4	2009-2008	10.00	7.94	7.81	10.00
5	2008-2007	11.57	10.43	8.36	10.62

Table A16: West Flower Garden Bank southeast-A core average annual extension across the slab orientations of 0°, 45°, 90° and 135° in mm/year.

Year	Estimated Time Interval	0°	45°	90°	135°
1	2012-2011	8.75	3.79	7.50	9.51
2	2011-2010	7.80	12.32	9.16	8.02
3	2010-2009	9.53	9.59	9.06	9.48
4	2009-2008	9.53	9.95	9.77	9.61
5	2008-2007	10.35	8.58	8.86	7.53

Table A17: West Flower Garden Bank southeast-B core average annual extension across the single 0.6mm slice orientations of 0°, 45° and 90° in mm/year.

Year	Estimated Time Interval	0°	45°	90°
1	2012-2011	0.15	6.06	3.77
2	2011-2010	8.47	7.49	7.12
3	2010-2009	8.93	10.85	12.87
4	2009-2008	10.11	9.83	9.81
5	2008-2007	10.16	10.37	11.55
6	2007-2006	8.47	11.75	7.48
7	2006-2005	9.75	9.71	10.32
8	2005-2004	10.55	5.94	10.32

Table A18: West Flower Garden Bank southeast-B core average annual extension across the slab orientations of 0°, 45° and 90° in mm/year.

Year	Estimated Time Interval	0°	45°	90°
1	2012-2011	0.15	0.96	3.29
2	2011-2010	8.42	8.39	8.50
3	2010-2009	9.03	9.11	9.28
4	2009-2008	9.96	9.77	9.93
5	2008-2007	10.32	10.43	9.64
6	2007-2006	8.32	8.39	8.68
7	2006-2005	9.96	9.95	10.47
8	2005-2004	10.55	9.98	10.32

Table A19: East Flower Garden Bank actual polyp annual extension rate in mm/year

Year	Estimated Time Interval	EFGB-NE	EFGB-SE	EFGB-SW
1	2012-2011	6.42	4.63	5.87
2	2011-2010	6.85	5.01	6.24
3	2010-2009	5.00	5.63	7.14
4	2009-2008	6.67	5.65	7.83
5	2008-2007	8.66	5.87	7.28
6	2007-2006	8.87	5.71	7.05
7	2006-2005	7.69	6.57	7.15
8	2005-2004	7.91	5.93	7.22
9	2004-2003	7.50	5.16	6.71
10	2003-2002	7.49	6.20	6.43
11	2002-2001		6.42	7.23
12	2001-2000		6.48	7.33
13	2000-1999			7.31
14	1999-1998			6.98
15	1998-1997			6.47
16	1997-1996			6.43
17	1996-1995			6.47
18	1995-1994			6.02
19	1994-1993			7.96

Table A20: West Flower Garden Bank actual polyp annual extension rate in mm/year

Year	Estimated Time Interval	WFGB-NE	WFGB-NW	W- SWA	W- SEA	W- SEB
1	2012-2011	4.90		4.92		
2	2011-2010	5.60	4.03	4.43	8.07	8.81
3	2010-2009	5.58	4.44	2.84	9.45	9.61
4	2009-2008	6.20	2.86	2.57	9.62	8.01
5	2008-2007	7.75	3.62	6.05	12.37	8.73
6	2007-2006	5.54	4.84	6.28		9.74
7	2006-2005	6.17	4.25	7.06		10.38
8	2005-2004	7.18	4.22	6.07		
9	2004-2003	6.89	4.22	7.23		
10	2003-2002	7.51	4.22	7.67		
11	2002-2001	9.16	6.05	6.07		
12	2001-2000		5.86			
13	2000-1999		3.87			
14	1999-1998		3.67			